Squeezed helical elastica

Lila Bouzar[a,b], Martin Michael Müller[c,d], Pierre Gosselin[e], Igor M. Kulić[d], Hervé Mohrbach[c,d]

a Département de Physique Théorique, Faculté de Physique,
USTHB, BP 32 El-Alia Bab-Ezzouar, 16111 Alger, Algeria
b Laboratoire de Physique et Chimie Quantique, Université Mouloud Mammeri, BP 17, 15000 Tizi-Ouzou, Algeria
c Equipe BioPhysStat, ICPMB-FR CNRS 2843, Université de Lorraine, 1 boulevard Arago, 57070 Metz, France
d Institut Charles Sadron, CNRS-UdS, 23 rue du Loess,
BP 84047, 67034 Strasbourg cedex 2, France and
e Institut Fourier, UMR 5582 CNRS-UJF, Université Grenoble I, BP74, 38402 Saint-Martin d'Hères, France

We theoretically study the conformations of a helical semi-flexible filament confined to a flat surface. This squeezed helix exhibits a variety of unexpected shapes resembling circles, waves or spirals depending on the material parameters. We explore the conformation space in detail and show that the shapes can be understood as the mutual elastic interaction of conformational quasi-particles. Our theoretical results are potentially useful to determine the material parameters of such helical filaments in an experimental setting.

PACS numbers: 82.35.Pq, 87.16.Ka

I. INTRODUCTION

Elastic objects exhibit a plethora of shapes in a confined geometry. Sometimes it requires a lot of imagination to deduce the original three-dimensional shape from the observation of its confined counterparts. In general, a geometrical confinement induces the breaking of a pre-existing symmetry of an elastic object. Soft matter physics offers many examples. For instance, a spherical membrane vesicle adopts an onion-like shape when confined inside a sphere of smaller size [1]. Elastic filaments in spherical confinement have been extensively studied, such as the morphology of a wire inside a cavity [2] or the shapes of semi-flexible filaments on a sphere [3]. A variation of the theme is the confinement of a polymer between two plates [4] or the morphology and dynamics of actin filaments osmotically confined to a flat surface [5]. Generally, one can find many more examples of rods confined to various two-dimensional surfaces in the literature [6–9].

In this paper we consider the planar confinement of a polymer which is not straight but helical in its ground state. Related problems were considered before like a twisted [10] or a nonlinearly elastic [11] rod under external loads confined on a plane. In living nature, one frequently finds helical polymers like microtubules [12, 13], Ftsz filaments [14] and dynamin [15]. Even whole microorganisms exhibit helicity inherited from their constituent filaments [16]. Different helically coiled structures have also been fabricated artificially such as coiled carbon [17] and DNA nanotubes [18]. To study these objects one often confines them to the focal plane of a microscope. This confinement changes the physical properties of the underlying objects and peculiar squeezed conformations often resembling looped waves, spirals or circles are observed [16–18]. Here we give an explanation for these observations. The helical filament is modeled as a semi-flexible polymer squeezed onto a flat surface and was previously called squeelix [19]. Excluded volume interactions are not taken into account in this approach, even though they are potentially relevant [9]. The variation of the linear elastic energy of the squeelix allows to determine the shapes at zero temperature. Varying the material parameters allows to classify the zoo of shapes in a manner similar to Euler elastica in three-dimensional space [20]. The results and the physical interpretation of the underlying theory are presented in the main text. The interested reader can find the mathematical details in the appendix.

In the following section we present the model and the fundamental equations of the squeelix elastica. In Sec. III we discuss the various shapes of a squeelix of infinite length. In this case these shapes are always ground states of the elastic energy. They can be understood qualitatively with the notion of conformational quasi-particles called twist-kinks [19]. These twist-kinks are another example of a general theme that we have already encountered in the context of microtubules [21]. In Sec. IV we will see that squeelices of finite length display a more complex behavior. The boundary conditions provoke the existence of metastable states which we will discuss in detail. In Sec. V we suggest a procedure how experimental data can be interpreted to extract material parameters from the theory.

II. A HELICAL WORM-LIKE CHAIN CONFINED IN TWO DIMENSIONS: THE SQUEELIX

A. Basic equations of the helical WLC model

The shape of an elastic rod can be described by the spatial evolution of the Frenet-Serret basis $(\mathbf{n}, \mathbf{b}, \mathbf{t})$ attached to the centerline of the rod. An internal twist of the rod is taken into account with the help of an additional local basis $(\mathbf{e}_1, \mathbf{e}_2, \mathbf{e}_3)$ which rotates with the material. This material frame or director basis $(\mathbf{e}_1, \mathbf{e}_2, \mathbf{e}_3)$ can be written in terms of the Frenet-Serret basis as $\mathbf{e}_3 = \mathbf{t}$, $\mathbf{e}_1 = \mathbf{n}\cos\psi + \mathbf{b}\sin\psi$ and $\mathbf{e}_2 = -\mathbf{n}\sin\psi + \mathbf{b}\cos\psi$, where ψ is the twist angle. The evolution of this basis along the centerline, described by the arc length s, is given by the twist equations $\mathbf{e}_i' = \mathbf{\Omega} \times \mathbf{e}_i$, where $\mathbf{\Omega} = (\Omega_1, \Omega_2, \Omega_3)$ is the strain vector function and $()'$ denotes the derivative with respect to s. The components of $\mathbf{\Omega}$ are [22]:

$$\Omega_1(s) = \kappa(s)\sin\psi(s) , \tag{1a}$$
$$\Omega_2(s) = \kappa(s)\cos\psi(s) , \tag{1b}$$
$$\Omega_3(s) = \tau(s) + \psi'(s) , \tag{1c}$$

where $\kappa(s) \geq 0$ and $\tau(s)$ are the local curvature and torsion, respectively. The local curvature is thus $\kappa^2(s) = \Omega_1^2 + \Omega_2^2$ and the twist density $\Omega_3(s)$ is the sum of the torsion and the excess twist ψ'.

For simplification, we consider an elastic rod of circular cross-section with a single bending modulus whose ground state is a helix in 3D space [33]. In linear elasticity theory, this helical worm-like chain minimizes the following energy:

$$E = \int \frac{B}{2}\left((\Omega_1 - \omega_1)^2 + (\Omega_2 - \omega_2)^2\right) + \frac{C}{2}(\Omega_3 - \omega_3)^2\, ds , \tag{2}$$

where B and C are the bending and torsional stiffness, respectively. The positive constant parameters ω_1 and ω_2 are the principal intrinsic curvatures and ω_3 the intrinsic twist. We consider a right-handed helix in the following, i.e., $\omega_3 > 0$. One can always set $\omega_2 = 0$ by a convenient choice of the material frame. The bending and the twist terms of the energy given by Eq. (2) can be minimized independently, yielding a curve of constant curvature $\kappa = \omega_1$ and torsion $\tau = \omega_3$. In the absence of an external torque there is no excess twist, $\psi' = 0$. This ground state is a helix of radius R and pitch H with

$$R = \frac{\omega_1}{\omega_1^2 + \omega_3^2} \qquad \text{and} \qquad H = \frac{2\pi\omega_3}{\omega_1^2 + \omega_3^2} , \tag{3}$$

satisfying the preferred curvature and twist everywhere. The components of the strain vector in the director basis can be expressed with the Euler angles $\varphi(s)$, $\theta(s)$ and $\psi(s)$ (see Fig. 1(a)):

$$\Omega_1 = \varphi'\sin\theta\sin\psi + \theta'\cos\psi , \tag{4a}$$
$$\Omega_2 = \varphi'\sin\theta\cos\psi - \theta'\sin\psi , \tag{4b}$$
$$\Omega_3 = \varphi'\cos\theta + \psi' . \tag{4c}$$

The curvature is then given by $\kappa^2(s) = \varphi'^2\sin^2\theta + \theta'^2$ and the torsion is $\tau = \varphi'\cos\theta$.

B. The squeelix

Confining the helical rod to the (xy) plane amounts to putting $\theta = \pi/2$. It is convenient to introduce the angle ϕ between the tangent of the centerline and the x axis defined as $\phi = \varphi - \pi/2$ (see Fig. 1(b)). Then, Eqs. (4) become

$$\Omega_1 = \phi'\sin\psi, \quad \Omega_2 = \phi'\cos\psi, \quad \Omega_3 = \psi' . \tag{5}$$

Hence the local curvature is simply given by $\kappa^2(s) = \phi'^2$ and the torsion $\tau = 0$ as the curve is now planar (see Fig. 1). The energy of a squeezed helical worm-like chain of length L (the so-called *squeelix*) can then be written as:

$$E = \frac{1}{2}\int_{-L/2}^{L/2}\left(B(\phi' - \omega_1\sin\psi)^2 + C(\psi' - \omega_3)^2 + B\omega_1^2\cos^2\psi\right) ds . \tag{6}$$

Note that under confinement the curvature and twist are now coupled. Minimizing E with respect to ϕ' gives
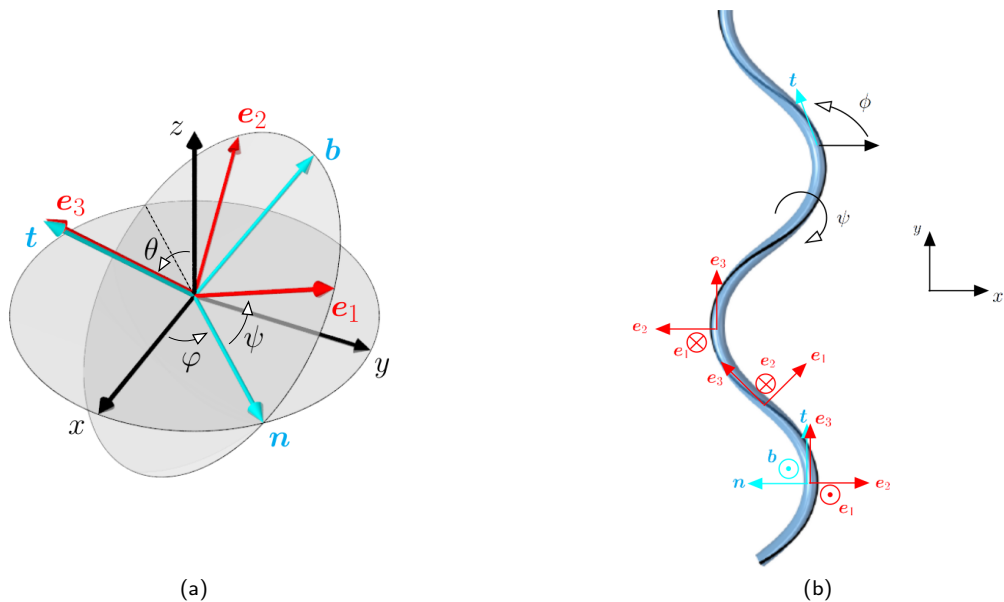
$$\phi' = \omega_1\sin\psi , \tag{7}$$

FIG. 1: (a) Representation of the Frenet-Serret basis, the director basis and the Euler angles at a position s of the centerline of a helical rod in three-dimensional space. The confinement onto the (xy) plane is realized by the projection of the tangent vector $\mathbf{t}$ (and thus $\mathbf{e}_3$) on that plane, $i.e.$, $\theta = \pi/2$. (b) Sketch of a confined helical rod with the two local bases. The Frenet-Serret vectors $\mathbf{n}$ and $\mathbf{t}$ evolve with s in the (xy) plane. The director vectors $\mathbf{e}_1$ and $\mathbf{e}_2$ attached to the material frame rotate in the $(\mathbf{nb})$ plane with an angle ψ when they evolve along the centerline. For the rest of this article the evolution of the vector $\mathbf{e}_2$ will be simply represented by a black ribbon drawn on the rod's surface (with $\mathbf{e}_2$ pointing in a direction perpendicular to the ribbon).

and Eq. (6) reduces to a functional of $\psi(s)$ alone

$$E[\psi] = \frac{1}{2} \int_{-L/2}^{L/2} \left(C \left(\psi' - \omega_3 \right)^2 + B\omega_1^2 \cos^2 \psi \right) ds \; , \tag{8}$$

for which the Euler-Lagrange equation is (see Appendix A):

$$\psi'' + \frac{B\omega_1^2}{2C} \sin(2\psi) = 0 \tag{9}$$

with free boundary conditions, $i.e.$, no torque at both ends of the filament

$$\psi'(-L/2) = \omega_3 = \psi'(L/2) \; . \tag{10}$$

Thus even in the absence of an external torque at the chain's ends, the confinement converts the intrinsic twist into an intrinsic torque. Eq. (9) is nothing less than the pendulum equation (with arc length s as the time and $\alpha = 2\psi$ the angle of the pendulum). Its solutions depend on the material parameters B, C, ω_1 and also ω_3 via the boundary conditions Eq. (10). The curvature $\kappa(s) = \phi'(s)$ of the squeelix can then be obtained directly from Eq. (7) . Note that in two dimensions the curvature can be negative. The fact that the curvature is slaved to the twist is the most important consequence of the squeezing of a helical WLC.

Integrating Eq. (9) we obtain

$$\psi'(s) = \pm \frac{1}{\lambda\sqrt{m}} \sqrt{1 - m \sin^2 \psi} \tag{11}$$

with λ a characteristic length scale given by

$$\lambda = \frac{1}{\omega_1} \sqrt{\frac{C}{B}} \tag{12}$$

and m a positive real parameter. The phase plane of Eq. (11) is well-known and the solutions of Eq. (9) are particular trajectories in this plane. A detailed discussion can be found in Appendix A. These solutions can be determined

numerically by integrating the differential equation (11). Alternatively, one can use the well-known explicit solution of Eq. (9). This will be very useful in the following since we want to compute the energy of the shapes of the squeelices, interpret them physically and discuss their stability.

The general solution of Eq. (9) such that $\psi(s_0) = 0$ is (see Appendix A)

$$\psi(s) = \pm am\left(\frac{s - s_0}{\lambda\sqrt{m}}\Big|m\right) \ , \tag{13}$$

where $am\,(x|m)$ is the elliptic Jacobian amplitude function whose behavior depends on the value m [23]. For the reader not familiar with elliptic functions, Figs. 3, 4, and 5 show the generic characteristic behavior of $\psi(s)$.

Squeelices are stable shapes if the second variation of E in Eq. (6) with respect to ϕ' and ψ at the extrema of the energy is positive definite. Writing $\phi' = \omega_1 \sin\psi + \delta\phi'$ we see that $\delta^2 E$ with respect to ϕ' gives the contribution $\frac{1}{2}\int_{-L/2}^{L/2} B\,(\delta\phi')^2\,ds$ which is positive definite. Therefore, the stability of squeelices relies on the sign of the second variation of $E[\psi]$ in Eq. (8). Note that integrals such as $E[\psi]$ never have maximisers (see, for instance, [11] and [24]). A solution (13) either leads to a stable squeelix if it is a local minimizer or to an unstable one if it is a saddle point of $E[\psi]$. This whole issue is discussed in detail in Appendix E.

An important remark is due here. The choice of the sign of $\psi(s)$ in Eq. (13) depends on the sign of ω_3. In this paper we have chosen $\omega_3 > 0$. This implies that $\psi'(-L/2)$ is positive as well. For $m < 1$ $\psi(s)$ is a monotonous function which then has to grow with s. For $m > 1$ $\psi(s)$ becomes a periodic function of s which has to grow in the vicinity of $-L/2$. Therefore, we have to choose the positive sign in Eq. (13) for all m.

By integrating the curvature, Eq. (7), we obtain $\phi(s)$, the angle between the tangent vector $\mathbf{t}$ and the x axis. We can then reconstruct the two-dimensional shapes in Cartesian coordinates with the relations:

$$x(s) = x_0 + \int_{-L/2}^{s} \cos\left(\phi(s')\right) ds' \ , \tag{14a}$$

$$y(s) = y_0 + \int_{-L/2}^{s} \sin\left(\phi(s')\right) ds' \ . \tag{14b}$$

The constants of integration m and s_0 have to be determined from the boundary conditions Eq. (10). For a chain of finite length L this problem turns out to be surprisingly complicated. But to grasp a physical intuition of the squeelix we first consider a very long chain where L is much larger than any characteristic length. In this case we can neglect the boundary conditions Eq. (10).

III.   SQUEELICES OF INFINITE LENGTH

A trivial solution of Eqs. (7) and (9) is $\psi = \pm\pi/2$ which corresponds to a shape of constant curvature $\kappa = \pm\omega_1$, i.e. multiple circles on top of each other. The energy density of this configuration is $E_0/L = C\omega_3^2/2$. The non-trivial general solution of Eq. (9) assuming the condition $\psi(0) = 0$ without loss of generality is thus:

$$\psi(s) = am\left(\frac{s}{\lambda\sqrt{m}}\Big|m\right) \ . \tag{15}$$

Therefore $\psi'(s) = \frac{1}{\lambda\sqrt{m}}dn\left(\frac{s}{\lambda\sqrt{m}}\Big|m\right)$ and $\psi'(0) = \frac{1}{\lambda\sqrt{m}}$. The curvature then reads

$$\kappa(s) = \omega_1 sn\left(\frac{s}{\lambda\sqrt{m}}\Big|m\right) \ , \tag{16}$$

where the functions dn, and sn are well-known elliptic Jacobian functions with parameter $m > 0$ [23]. The function sn is a periodic odd function of amplitude unity whose period is $l_p = 4\lambda\sqrt{m}\mathcal{K}(m)$, where $\mathcal{K}(m)$ denotes the complete elliptic integral of the first kind.

From Eqs. (14a), (14b) and (16) all shapes can be determined. There is an infinite number of solutions since we do not impose the boundary conditions Eq. (10). This set of solutions splits into two categories, the oscillatory and the revolving regimes of the pendulum which correspond to $m > 1$ and $m < 1$, respectively. The limiting case $m = 1$ is the homoclinic pendulum that has just enough energy to make one full $\alpha = 2\pi$ (or $\psi = \pi$) rotation in an infinite "time" interval. This ensemble of solutions leads to a variety of shapes resembling loops, waves, spirals or circles that we are going to explore.

A. The energy density of a squeelix

To each value of the parameter m corresponds a different filament shape. But a helical filament of length L with material parameters B, C, ω_1 and ω_3 will adopt a single ground state when squeezed into the plane. This shape is the one minimizing the total elastic energy E of the chain. In order to compare the energy of the various solutions in the limit large L we only need compute the energy per length $e = E/L$ given by (see Appendix B)

$$e(m) = \frac{\omega_1 \sqrt{BC}}{L\sqrt{m}} \left(\mathcal{E}\left(\psi\left(L/2\right)|m\right) - \mathcal{E}\left(\psi\left(-L/2\right)|m\right)\right) + \frac{B\omega_1^2}{2}\left(1 + \frac{1}{\mu} - \frac{1}{m}\right) - \frac{C\omega_3}{L}\left(\psi\left(L/2\right) - \psi\left(-L/2\right)\right) \quad (17)$$

with $\mathcal{E}\left(x|m\right)$ the elliptic integral of the second kind [23], and

$$\mu = \frac{\omega_1^2 B}{\omega_3^2 C} = \frac{\pi^2}{4}\gamma \,, \quad (18)$$

which measures the ratio of the bending energy $\propto B\omega_1^2$ over the twist energy $\propto C\omega_3^2$. The control parameter

$$\gamma = \frac{4\omega_1^2 B}{\pi^2 \omega_3^2 C} \quad (19)$$

will play a crucial role in the following. To simplify the analysis of the energy density, we consider the two different behaviors of the pendulum separately.

For the oscillating pendulum ($m > 1$) we consider the energy per period since $E/L = E_p/l_p$ with E_p the energy of one period of oscillation and $l_p = 4\lambda\mathcal{K}\left(\frac{1}{m}\right)$. Using $\psi\left(l_p/2\right) = \psi\left(-l_p/2\right)$ we obtain the energy density

$$e_{m>1}(m) = \frac{B\omega_1^2}{2}\left(1 + \frac{1}{\mu} - \frac{1}{m}\right) \,, \quad (20)$$

which is a monotonously growing function of m. Its minimum at $m = 1$ is given by

$$e_{m=1} = \lim_{L \to \infty} \frac{E}{L} = \frac{1}{2}C\omega_3^2 = E_0/L \,, \quad (21)$$

which is degenerate with the energy density of the trivial solution of constant curvature. The absence of minima for all $m > 1$, implies that the associated shapes cannot be a ground state of a squeelix of infinite length.

In the case of the revolving pendulum ($m < 1$) we compute the energy per length by using $E/L = E_{cycle}/l_{cycle}$ with E_{cycle} the energy for a single cycle defined by the condition $\psi(s + l_{cycle}) = \psi(s) + \pi$ with

$$l_{cycle}/\lambda = 2\sqrt{m}\mathcal{K}(m) \,. \quad (22)$$

Since $\psi(l_{cycle}/2) = \psi(-l_{cycle}/2) + \pi$ we have $\mathcal{E}\left(\psi\left(l_{cycle}/2\right)|m\right) - \mathcal{E}\left(\psi\left(-l_{cycle}/2\right)|m\right) = 2\mathcal{E}(m)$ where $\mathcal{E}\left(m\right)$ is the complete elliptic integral of the second kind [23]. The energy density becomes

$$e_{m<1}(m) = \frac{B\omega_1^2}{m}\frac{\mathcal{E}(m)}{\mathcal{K}(m)} + \frac{1}{2}B\omega_1^2\left(1 + \frac{1}{\mu} - \frac{1}{m}\right) - \frac{\pi\sqrt{BC}}{2}\frac{\omega_1\omega_3}{\sqrt{m}\mathcal{K}(m)} \,. \quad (23)$$

Remarkably, $e_{m<1}(m)$ exhibits a minimum at $m = m^*$ given by the equation

$$\frac{\sqrt{m^*}}{\mathcal{E}(m^*)} = \sqrt{\gamma} \,. \quad (24)$$

Note that $\sqrt{m}/\mathcal{E}(m) \leq 1$ for all $m \leq 1$. Thus, this minimum only exists for $\gamma \leq 1$.

Eq. (24) shows that the ground state of a squeelix of infinite length is determined by the parameter γ. For $\gamma < 1$, the ground state is given by the set of equations Eqs. (14a), (14b) and (16). The parameter m in these equations is the solution of Eq. (24) and is therefore smaller than unity (revolving pendulum). For small values $\gamma \ll 1$, we find $m^* \approx \frac{\pi^2}{4}\gamma = \mu$. When γ is approaching unity $\gamma \lesssim 1$ we see that $m^* \approx \gamma$. For $\gamma > 1$ the minimum of $e_{m<1}(m)$ is at $m = 1$ with $e_{m<1}(1) = E_0/L = e_{m>1}(1)$. To illustrate our findings, Fig. 2 shows the energy density as a function of m for different values of γ. Figures 3-5 show a variety of possible shapes depending on the material parameters.

The parameter γ allows to make a connection between these shapes and the three-dimensional unconfined helix. From Eqs. (3) and (19) one obtains the ratio between pitch and radius of the helix as $\frac{H}{R} = 4\sqrt{\frac{B}{C}}\frac{1}{\sqrt{\gamma}}$. In the regime $\gamma \gg 1$, the pitch of the unconfined 3D helix is much smaller than its radius, $H \ll R$, which translates to a circular squeelix after confinement onto the plane. In the opposite regime $\gamma \ll 1$, where the helix is extended ($H \gg R$), the confinement leads to other, nontrivial shapes with $m < 1$. To understand these shapes in more detail we are now going to study the squeelix in terms of entities that we call twist-kinks.
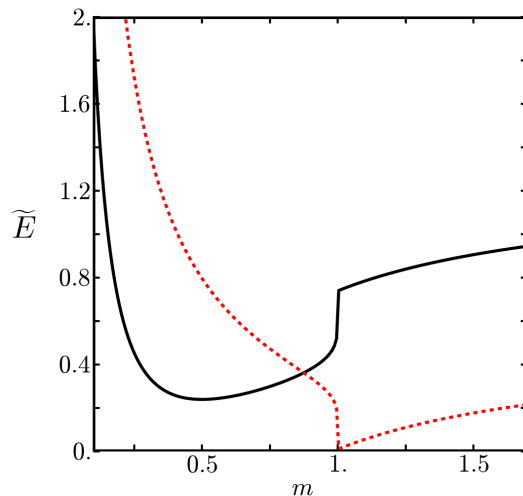
FIG. 2: Scaled energy density $\widetilde{E} = E/(B\omega_1^2 L)$ of a squeelix of infinite length for $\gamma = 0.274$ with $C/B = 1$ and $\omega_3/\omega_1 = 1.22$ (black solid curve). The minimum of this curve lies at $m^* = 0.5$ as predicted by Eq. (24). For $\gamma > 1$ the minimum of the scaled energy is at $m^* = 1$ as exemplified by the red dotted curve where $\gamma = 20.26$ with $C/B = 1$ and $\omega_3/\omega_1 = 0.14$.
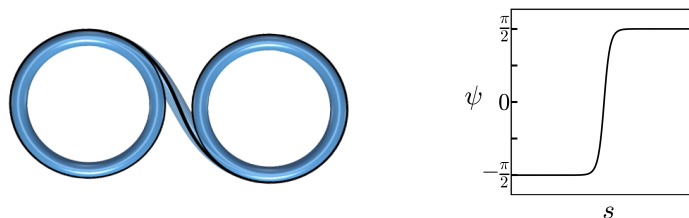

FIG. 3: Squeelix of infinite length for $m = 1$ (left) and its twist $\psi(s)$ (right). The shape contains only a single twist-kink of size λ. Lengths are given in units of ω_1^{-1}. In this example $\sqrt{C/B} = 1$, $\omega_3 = 0.64\omega_1$, $\lambda = 1$ and $\gamma = 1$.

B. The twist-kink picture

The solutions describing the ground state of the squeelix in terms of elliptic Jacobi functions are not very illuminative. To gain more physical insight we will use the concept of a twist-kink introduced in Ref. [19]. This object corresponds to a region of the filament where the twist is highly concentrated and the curvature flips. A squeelix can be interpreted as the result of the elastic interaction between twist-kinks along the filament. Mathematical details are provided in Appendix C.

1. The homoclinic pendulum ($m = 1$)

A filament with a *single* twist-kink only exists for $m = 1$. Eq. (15) becomes the Gudermann function $\psi(s) = gd\,(s/\lambda)$ which also reads

$$\psi(s) = 2\arctan(e^{s/\lambda}) - \pi/2 \,. \tag{25}$$

This configuration interpolates between $\psi(-\infty) = -\pi/2$ and $\psi(\infty) = \pi/2$ where the curvatures are opposite, *i.e.*, $\kappa(\pm\infty) = \pm\omega_1$. The region of the filament of size λ where the twist is highly concentrated and where the curvature

$$\kappa(s) = \omega_1 \tanh(s/\lambda) \tag{26}$$
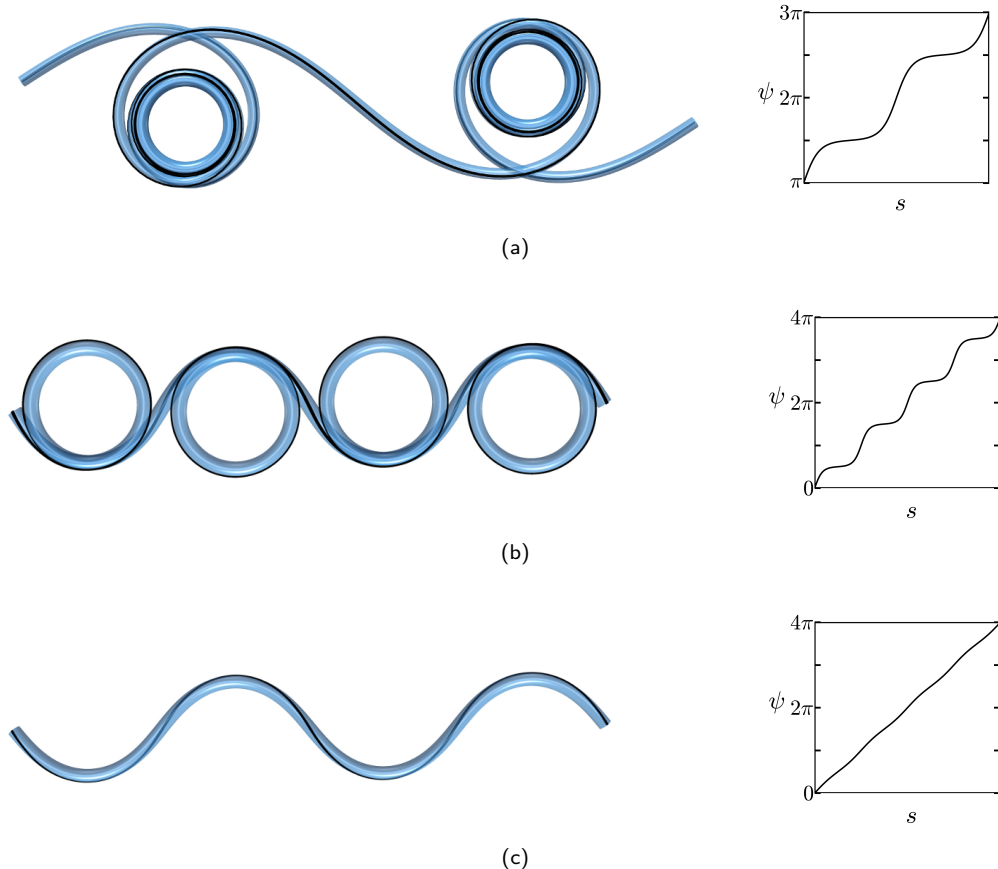
(a)

(b)

(c)

FIG. 4: Finite sections of the shapes of squeelices of infinite length in their ground state (left) and the associated twist $\psi(s)$ (right) for $m < 1$. Lengths are given in units of ω_1^{-1} and $l_{loop} = 2\pi\omega_1^{-1}$. For γ close to one typical shapes are either circular or spiral windings depending on the ratio l_{cycle}/l_{loop}. For instance, in (a) and (b) we have set $\gamma = 0.995$ for which $m = 0.999$. In (a) we have set $\sqrt{C/B} = 10$ so that $\omega_3 \approx 0.06\omega_1$, $\lambda \approx 10.0\omega_1^{-1}$, and $l_{cycle} \approx 96.8\omega_1^{-1} \gg l_{loop}$. In (b) we have decreased $\sqrt{C/B}$ to one so that $\omega_3 \approx 0.64\omega_1$, $\lambda \approx 1.0\omega_1^{-1}$, and $l_{cycle} \approx 9.7\omega_1^{-1}$ which is of the order of l_{loop}. (c) For $\gamma = 0.274$ one finds $m = 0.5$. This corresponds to the dense twist-kink regime where the shape is sinus-like and the twist grows approximately linearly with s. The parameters of this example are $\sqrt{C/B} = 1$ and thus $\omega_3 \approx 1.22\omega_1$, $\lambda \approx 0.7\omega_1^{-1}$, and $l_{cycle} \approx 2.6\omega_1^{-1}$.

flips (curvature inversion points) was called a *twist-kink* in Ref. [19] in analogy to the concept of kinks in soliton physics [25]. Since $\lambda/L \ll 1$ the filament consists of two regions of approximately constant opposite curvature $\kappa \approx \pm\omega_1$ separated by a region of size λ (see Fig. 3).

The energy of this chain is $E_1 = 2\sqrt{BC}\omega_1 - \pi C\omega_3 + C\omega_3^2 L/2$. Therefore, the self-energy of a single twist-kink is

$$\Delta E = E_1 - E_0 = \pi C\omega_3(\sqrt{\gamma} - 1) , \tag{27}$$

where γ can now be interpreted as a *twist-kink expulsion parameter* [19]. This terminology speaks for itself: for $\gamma > 1$ the twist-kink is expelled from the filament, which consequently forms superimposed circles of radius $1/\omega_1$. For $\gamma < 1$, the squeelix can by populated by twist-kinks whose density is limited by their repulsive interactions.

2. The revolving pendulum ($m < 1$)

In a revolving pendulum the twist angle $\psi(s)$ is a monotonously growing function of s. The length l_{cycle} is given by the condition $\psi(s + l_{cycle}) = \psi(s) + \pi$. As a consequence of Eq. (7) the curvature of the filament reverses its sign every l_{cycle}, i.e., $\kappa(s + l_{cycle}) = -\kappa(s)$. Depending on the ratio l_{cycle}/λ the squeelix adopts different typical periodic shapes.

When $l_{cycle}/\lambda \gg 1$, we are in a regime where $m \lesssim 1$ since the expansion of Eq. (22) gives $l_{cycle}/\lambda \approx \ln(\frac{16}{1-m})$ at lowest order. For instance, one obtains $l_{cycle}/\lambda \geq 10$ for $m \geq 0.999$. In this regime Eq. (24) implies that $m \approx \gamma$. The ground
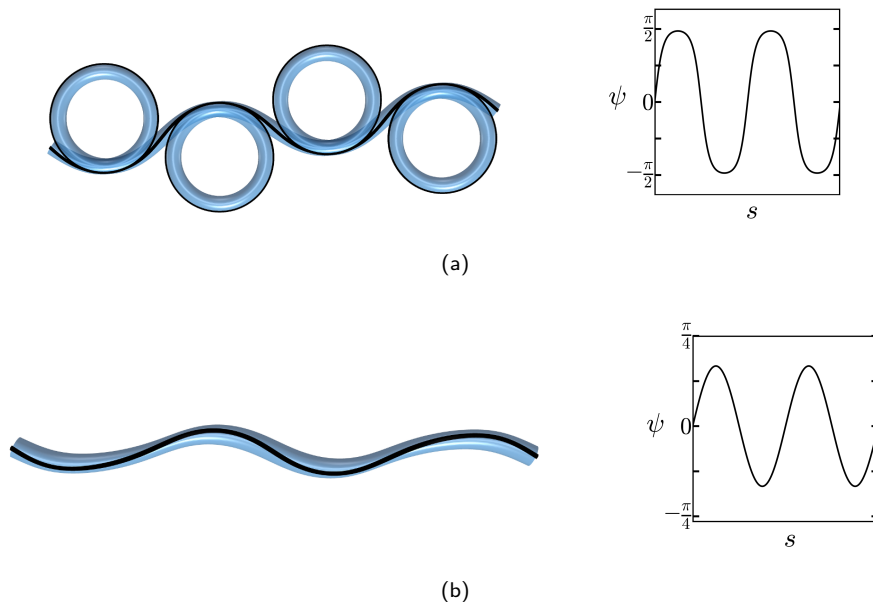
(a)

(b)

FIG. 5: Finite sections of the shapes of squeelices of infinite length (left) and the associated twist $\psi(s)$ (right) for $m > 1$. Lengths are given in units of ω_1^{-1} and $l_{loop} = 2\pi\omega_1^{-1}$. These shapes do not minimize the energy density and are thus independent of γ. (a) Squeelix with $m = 1.002$ and $\sqrt{C/B} = 1$, and thus $l_{period} \approx 18\omega_1^{-1} \gg l_{loop}$. (b) Squeelix with $m = 4$ and $\sqrt{C/B} = 1$, and thus $l_{period} \approx 7\omega_1^{-1}$, which is of the same order of magnitude as l_{loop}.

state of the filament is populated by a low density $\rho \simeq 1/l_{cycle}$ of twist-kinks of the form $\psi(s) \approx gd\,(s/\lambda) + O(1-m)$. The density is limited by the mutual kink-kink repulsion $U_{int} \sim \pi C \omega_3 \sqrt{\gamma} e^{-d/\lambda}$ for $d/\lambda \gg 1$, where d is the distance between the two entities (see Appendix C).

One finds three types of behavior depending on the ratio l_{cycle}/l_{loop} where $l_{loop} = \frac{2\pi}{\omega_1}$ is the length of a loop of constant radius ω_1. When $l_{cycle} \gg l_{loop}$ the shape of the squeelix consists of a succession of spiral windings with minimal radius of curvature $1/\omega_1$ and alternating sign of curvature, Fig 4(a). The twist-kinks are localized at the curvature inversion points. When $l_{cycle} \approx l_{loop}$ each loop has only one turn Fig 4(b). Finally, for $l_{cycle} < l_{loop}$ the shape consists of a succession of flipped circular arcs (incomplete loops) separated by the twist-kinks.

When l_{cycle} is of the same order or smaller than λ, no loops are formed and the shape of the filament is sinus-like Fig 4(c). The density of twist-kinks is very high. The more l_{cycle}/λ is decreased the more the twist-kinks are deformed up to the point where the notion of individual twist-kinks looses its meaning. In the limit $m \ll 1$, the twist evolves linearly $\psi(s) \approx \frac{\pi}{l_{cycle}}s$ with $l_{cycle} \approx \lambda\pi\sqrt{m}$ and the curvature is given by $\kappa(s) \approx \omega_1 \sin(\frac{\pi}{l_{cycle}}s)$. This explains the sinus-like shape of the squeelix. The number of curvature inversion points per unit length (previously identified as the density of twist-kinks) is given by $\rho \simeq 1/l_{cycle} = \omega_3/\pi$ (see Appendix D). Therefore, $m \approx \frac{\pi^2}{4}\gamma$, which implies that γ is small in this regime.

3. The oscillating pendulum ($m > 1$)

Although the shapes do not minimize the energy density in this regime, we nevertheless consider them for completeness. Moreover, we will see in the next section that similar shapes are local energy minima when the length of the squeelix is finite.

When $m > 1$, the twist angle $\psi(s)$ oscillates periodically between two values $[-\psi_0, \psi_0]$ with $\psi_0 = \arcsin(1/\sqrt{m})$ over an arc length $l_{cycle} = 2\lambda K\left(\frac{1}{m}\right)$. The curvature, Eq. (16), can be written as

$$\kappa(s) = \frac{\omega_1}{\sqrt{m}} sn\left(\frac{s}{\lambda}\bigg|\frac{1}{m}\right) \ . \tag{28}$$

It is a periodic function of period $l_p = 2l_{cycle}$ with maximal curvature $\kappa_0 = \pm\omega_1/\sqrt{m}$.

In the regime $l_{cycle}/\lambda \gg 1$ where $m \gtrsim 1$, the formation of loops depends again on the ratio l_{cycle}/l_{loop}. The shape of the squeelix contains a low density of alternating twist-kinks and anti-twist-kinks. With decreasing l_{cycle}/λ or

increasing m, the curvature becomes $\kappa(s) \approx \frac{\omega_1}{\sqrt{m}} \sin\left(\frac{s}{\lambda}\right) + O(1/m)$ with decreasing amplitude. The shape is sinus-like as well. The reason why this solution is not the ground state of a squeelix is due to the fact that the anti-kink has $\psi'(s) < 0$ around the curvature inversion point. This maximizes the purely twist energy contribution to the total energy. Fig. 5 show two typical shapes.

IV. SQUEELICES OF FINITE LENGTH

The case of a squeelix of infinite length whose structure repeats itself allowed us to grasp a physical intuition of the system. But in the real world, filamentous objects always have a finite size. We are now going to study the more realistic case of a filament of finite length L in detail. The major difference is that for infinite length, the density of twist-kinks is determined by their mutual repulsion which depends only on the material parameters. For the finite case there is the additional constraint that the twist-kinks must fit inside the chain. Their density will thus depend on L. Our goal is to study all these solutions and give them a physical sense. Here we will focus only on the main results as the mathematical details are provided in Appendices C, D and E.

A. Basic equations

For a filament of finite length L, the general solution of Eq. (9) reads

$$\psi(s) = am\left(\frac{s - s_0}{\lambda\sqrt{m}} \middle| m\right) \tag{29}$$

with the arc length s_0 such that $\psi(s_0) = 0$ (see Section II B). Importantly, this solution must satisfy the boundary conditions Eq. (10)

$$\psi'(-L/2) = \omega_3 = \psi'(L/2) \tag{30}$$

with

$$\psi'(s) = \frac{1}{\lambda\sqrt{m}} dn\left(\frac{s - s_0}{\lambda\sqrt{m}} \middle| m\right) . \tag{31}$$

Plugging Eqs. (29) and (31) into the expression of the energy, Eq. (17), leads to the energy $E(m, s_0)$ for a given length L as shown in Fig. 11 of Appendix D. The energy $E(m, s_0)$ is defined on a subspace of the functional space of the energy $E[\psi]$ in Eq. (8). We observe an energy landscape with many localized minima, maxima and saddle points. Integrating Eq. (31) from s_0 to $-L/2$ leads to

$$s_0 = -\frac{L}{2} - \lambda\sqrt{m}\mathcal{F}\left(\psi(-L/2) \middle| m\right) , \tag{32}$$

where $\mathcal{F}(x|m)$ is the elliptic integral of the first kind [23]. As shown in Appendix A one obtains

$$\psi\left(-L/2\right) = \pm \arcsin\left(\sqrt{\frac{1}{m} - \frac{1}{\mu}}\right) + n\pi \tag{33}$$

with $n = 0, 1$, as a consequence of Eq. (30). These two cases are related by the transformation $\psi(s) \to \psi(s) + \pi$. They lead to two shapes related by the transformation $\kappa(s) \to -\kappa(s)$. These two shapes have thus the same energy. We therefore consider the case $n = 0$ only. Thus $-\pi/2 < \psi\left(-L/2\right) < \pi/2$ and

$$\frac{\mu}{1 + \mu} \leq m \leq \mu \tag{34}$$

with $\mu = \frac{\omega_1^2 B}{\omega_3^2 C}$. We still have to determine the values of m associated to the extrema of the energy. But first it is interesting to treat s_0 as a function of m. This leads to two different trajectories $s_{0,\pm}(m)$ on the energy surface $E(m, s_0)$ depending on the sign of $\psi\left(-L/2\right)$ in Eq. (33). In Appendix D it is shown that the trajectory $s_{0,+}(m)$ connects saddle points to minima of the energy landscape $E(m, s_0)$ whereas $s_{0,-}(m)$ connects maxima to saddle points. As we will see the local maxima and saddle points of $E(m, s_0)$ are also saddle points of the energy $E[\psi]$ (the latter having no local maximizers) and thus they lead to unstable squeelices. Although it appears possible that some
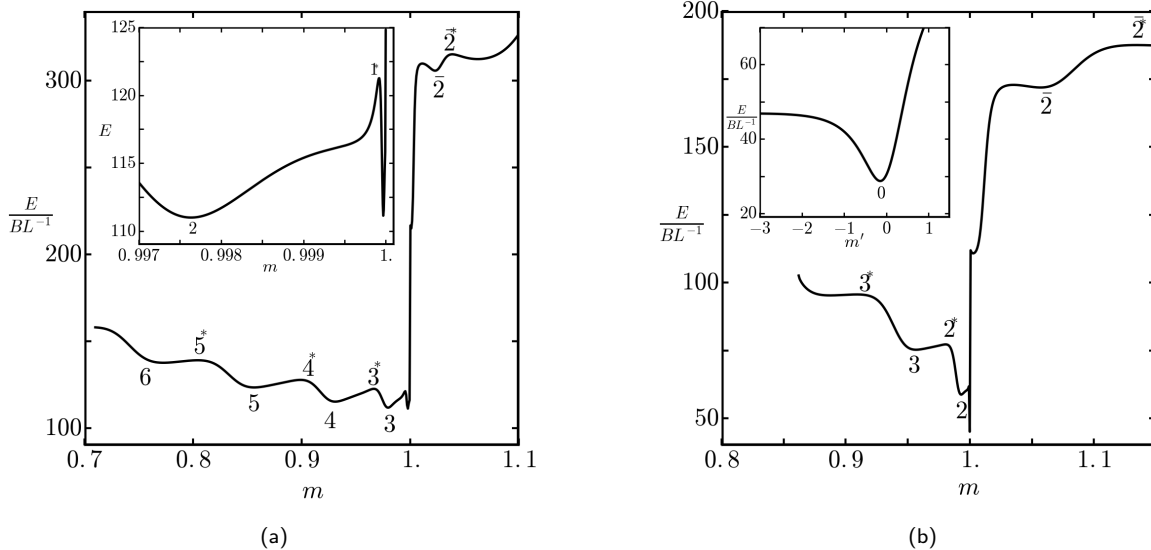
(a)

(b)

FIG. 6: Energy $E(m, s_{0,+}(m))$ as a function of m for different values of γ. Energies and lengths are measured in units of BL^{-1} and L, respectively. We set $\sqrt{C/B} = 1$. For $m < 1$ the integer n denotes the energy minima of squeelices with n twist-kinks and n^* denotes the energy barriers corresponding to unstable critical shapes. The notation $\bar{n}$ and $\bar{n}^*$ are used for the local minima and maxima respectively in the region $m > 1$. In this region some of the extrema are not numbered since they do not satisfy the boundary conditions, Eq. (10) (see the explanation in the main text). (a) Energy $E(m, s_{0,+}(m))$ for $\gamma = 0.9915$ with $\omega_1 = 24.4L^{-1}$ and $\omega_3 = 15.6L^{-1}$. The ground state corresponds to the minimum 2 as shown in the inset. In this state the squeelix has two twist-kinks. The minima near $m = 1$ (states $n = 0$, $n = 0^*$ and $n = 1$) are too close to each other to be distinguishable at this scale (first minimum, not numbered). (b) Energy for $\gamma = 2.5330$, $\omega_1 = 20L^{-1}$ and $\omega_3 = 8L^{-1}$. In this regime the ground state is the state without twist-kink (the state denoted 0) as shown in the inset where we introduced $m' = (m - 1) \cdot 10^8$ for convenience. A finite number of local minima with various numbers of twist-kinks exists. The states 0^*, 1 and 1^* are not distinguishable in the figure. In both cases (a) and (b) the states $\bar{1}$ and $\bar{1}^*$ are not distinguishable as well.

of the local minima of $E(m, s_0)$ are saddle points of $E[\psi]$, this is in fact not the case. All minima of $E(m, s_0)$ are minima of $E[\psi]$ and their corresponding shapes are consequently stable (see Appendix E). The approach through the introduction of the energy $E(m, s_0)$ will allow us to give a physical understanding of all these extremal shapes.

To obtain the energy minima $E(m, s_0(m))$, we focus on the case $s_{0,+}(m)$ in the following. Fig. 6 shows the function $E(m, s_{0,+}(m))$ for different values of γ. One finds that the global minimum lies in the interval $0 < m < 1$ for all values of γ. In the regime of weak γ the local minima with $m < 1$ are lower than the local minima with $m > 1$. These configurations are thus less accessible at finite temperature. For increasing $\gamma \lesssim 1$, the local minima for both $m < 1$ and $m > 1$ can have comparable energies, and the global minimum approaches $m = 1$ from below. Note, however, that it is only equal to one in the infinite case. In the opposite regime $\gamma \gg 1$ local minima with $m > 1$ are lower than the local minima with $m < 1$. What are the typical shapes of these extrema?

B. Shapes of squeelices of finite length

We must again separate the study in two parts. While we focus on the main points in this section, we refer to Appendix D for more details on the mathematical derivation.

1. The revolving pendulum ($m < 1$)

A revolving pendulum with the boundary conditions $\psi'(-L/2) = \omega_3 = \psi'(L/2)$ must satisfy either

$$\psi(L/2) = \psi(-L/2) + n_a\pi \quad \text{(case (a))} \qquad \text{or} \tag{35a}$$
$$\psi(L/2) = -\psi(-L/2) + n_b\pi \quad \text{(case (b))} . \tag{35b}$$

As discussed in the previous section we focus primarily on $\psi\left(-L/2\right) > 0$, $i.e.$, the case $s_{0,+}$. The integers $n_{a,b} \geq 1$ cannot exceed a maximum value which depends on the chain length L and the twist-kink repulsion. The solutions of case (a) and (b) correspond to the maxima and minima of the energy $E(m, s_{0,+}(m))$, respectively, as shown in Fig. 6. Intuitively, the minima correspond to symmetric shapes (with respect to the center of the chain at $s = 0$) with $n_b - 1$ twist-kinks disposed along the chain in an equidistant manner. These shapes are stable, $i.e.$, minimizers of $E[\psi]$ (see Appendix E). The ground state $n_b = n_b^*$ results from the optimal combination of the twist-kink self-energy (when it is negative) and the repulsive energy between them.

It is appealing to look at simple shapes associated to the states of Fig. 6. When $n_b = 1$, the shape is a circular arc without twist-kinks, whereas $n_a = 1$ corresponds to a curvature inversion point or a partial twist-kink localized near the end of the chain at $s = L/2$. This is the critical configuration on the top of the energy barrier of $E(m, s_{0,+}(m))$ that the system must exceed in order to reach the next minimum with $n_b = 2$. The corresponding shape contains a single twist-kink in the middle of the chain. The procedure for higher n follows the same behavior. Therefore, asymmetric shapes with a curvature inversion point, that we call a critical twist-kink, localized at $s = L/2$ correspond to case (a). They are the critical shapes on top of the energy barrier of $E(m, s_{0,+}(m))$ that must be overcome to inject (or remove) an additional twist-kink into the chain in order to reach the next local minimum (see Fig. 7). These critical asymmetric shapes are unstable.

To come back to the case $s_{0,-}$ note that a solution of case (a) with $s_{0,-}$ leads to a shape which is almost identical to its $s_{0,+}$ counterpart, except that the curvature inversion point that is localized at $s = L/2$ for $s_{0,+}$ is localized at $s = -L/2$ (see Appendix D for more details). In other words, the shape contains a critical twist-kink symmetrically localized at the opposite end of the chain. Since it costs the same energy to add a twist-kink from one end or the other end of the chain, both shapes have the same elastic energy.

A solution of case (b) with $s_{0,-}$ turns out to be an energy maximum of $E(m, s_{0,-}(m))$ with a critical twist-kink at each of the two ends. For this reason its energy is even higher than the energy of the equivalent maximum of case (a) with $s_{0,+}$. The trajectory $s_{0,-}(m)$ thus passes through states which contain either one or two critical twist-kinks.

In summary, the shapes having either one critical twist-kink near one end of the chain, $i.e.$, case (a) of the trajectories $s_{0,+}$ and $s_{0,-}$ or two critical twist-kinks at both ends, $i.e.$, case (b) of the trajectory $s_{0,-}$, are all unstable. Examples are provided in Fig. 8.

2. The oscillating pendulum $(1 < m < \mu)$

In this regime we have the following two boundary conditions

$$\psi\left(L/2\right) = \psi\left(-L/2\right) \quad \text{(case (a))}, \tag{36a}$$

$$\psi\left(L/2\right) = -\psi(-L/2) \quad \text{(case (b))}, \tag{36b}$$

which corresponds to equal (a) or opposite (b) curvatures at the ends of the squeelix. The cases (a) and (b) correspond to the local maxima and minima of the energy $E(m, s_{0,+}(m))$, respectively. In Appendix E it is shown that only the solutions of case (b) with $\psi(-L/2) > 0$ (trajectory $s_{0,+}$) are stable. Therefore, as for $m < 1$ we focus mainly on the trajectory $s_{0,+}$. In case (a) the boundary conditions Eq. (30) imply that $L = l_p n_a$ with the integer $n_a \geq 1$ and $l_p(m)$ the period of oscillations.

For a given n_a there are thus $2n_a$ curvature inversion points (where $\psi\left(s\right) = 0$). However, the last one is close to the end of the chain $s = L/2$. This shape is asymmetric with respect to the center of the chain. Similarly to the case of the revolving pendulum it is the critical shape on top of the energy barrier that must be overcome to reach the next minimum of $E(m, s_{0,+}(m))$, $i.e.$, a shape of type (b). In contrast to before one now has to add or remove an anti-twist-kink at the end of the chain. The shapes of case (b) are symmetrical with respect to $s = 0$ as their curvature inversion points are equidistant along the chain (see Fig 7). They are minimizer of $E[\psi]$ and are stable.

The solutions of case (a) are again related to their counterpart with $s_{0,-}$ and have the same energy (details in Appendix D). They are critical shapes with a curvature inversion point (close to the origin of the chain for $s_{0,-}$, and close to its end for $s_{0,+}$) on top of the energy barrier of $E(m, s_{0,+}(m))$.

Case (b) with $s_{0,-}$ is an energy maximum as the shapes contain two curvature inversion points near each end of the chain. These configurations again have a much larger energy than the equivalent maximum of case (a) with $s_{0,+}$.

The shapes having either one critical anti-twist-kink (curvature inversion point) near one end of the chain, $i.e.$, case (a) of the trajectories $s_{0,+}$ and $s_{0,-}$ or two critical anti-twist-kinks at both ends, $i.e.$, case (b) of the trajectory $s_{0,-}$, are all unstable. Two examples with a single critical anti-twist-kinks can be seen in Fig. 9.

Fig. 6 shows the energy $E(m, s_{0,+}(m))$ for different values of γ. The corresponding trajectories $s_{0,+}(m)$ are solutions of the Euler-Lagrange equations with $\psi'(-L/2) = \omega_3$. They pass by the extrema we are searching for, $i.e.$, which fulfill the boundary conditions at both ends, Eq. (10). For $m > 1$ these trajectories also exhibit other extrema m_i

which do not satisfy $\psi'(L/2) = \omega_3$ but are nevertheless extrema $\delta E = 0$ as the corresponding boundary term in Eq. (A4) vanishes due to $\delta\psi(L/2)\big|_{m_i} = \frac{\partial\psi(L/2)}{\partial m}\big|_{m_i}\delta m = 0$. Even though $s_{0,+}(m)$ passes by all local extrema one can find other trajectories $s(m)$ which do not satisfy the boundary conditions but have a lower energy for a given m (not shown in Fig. 6).

3. Finding the ground state

As we have seen, choosing the material parameters such that the *twist-kink expulsion parameter* $\gamma > 1$ leads to a ground state with zero twist-kinks. The twist ψ of this ground state is given by a Jacobi amplitude function with a value $m = \underline{m}$ very close but smaller than 1. An example is given by the state 0 in Fig. 6 where $\underline{m} = 0.9999999985$. This state satisfies the condition $\psi(L/2) = -\psi(-L/2) + \pi$ (cf. Eq. (35b) with $n_b = 1$) with $0 < \psi(-L/2) = \arcsin\left(\sqrt{1/\underline{m} - 1/\mu}\right) < \pi/2$. The shape of the filament is a circular arc of curvature $\kappa = \omega_1$ in its bulk with deformed ends. This ground state is obviously degenerate with the symmetric shape $\kappa = -\omega_1$ corresponding to the transformation $\psi(s) \to \psi(s) + \pi$.

For $\gamma < 1$, the injection of twist-kinks is favored and the theory predicts the existence of many metastable (and unstable) states with a different number of twist-kinks within the filament. The energy of these states consists of two terms. The negative self-energy of the twist-kinks and their positive mutual interaction which also includes the repulsion between the twist-kinks and the partial twist-kinks at the chain ends. The global minimum of the energy is reached for an optimal number of twist-kinks that makes the best compromise between the two contributions of the energy.

For each value of m corresponding to a local minimum of the energy $E(m, s_{0,+}(m))$ there is a state satisfying Eq. (35b) and having $n_b(m) - 1$ twist-kinks. These states satisfy the relation

$$L = l_{cycle}(m)n_b(m) - 2\Delta s(m) \tag{37}$$

with $\Delta s(m) = -L/2 - s_{0,+}(m) = \lambda\sqrt{m}\mathcal{F}(\psi(-L/2)|m)$ and $l_{cycle} = 2\lambda\sqrt{m}\mathcal{K}(m)$. Thus the number of twist-kinks associated to this state is given by:

$$n_b(m) = \frac{L + 2\Delta s(m)}{l_{cycle}(m)} . \tag{38}$$

For each integer $n_b = 1, 2, \ldots$ there is an associated value of m corresponding to a local minimum of the energy. The case $n_b = 0$ is relevant for very short length L only (see Appendix D) and is not considered in the main text. The function $n_b(m)$ is decreasing with $m \in [\mu/(1+\mu), \underline{m}]$. The maximum number of twist-kinks within the filament or equivalently the number of metastable states n_{max} is

$$n_{max} = \left\lfloor n_b\left(\frac{\mu}{1+\mu}\right)\right\rfloor - 1 = \left\lfloor\frac{L}{l_{cycle}(\mu/(1+\mu))}\right\rfloor , \tag{39}$$

where $\lfloor x\rfloor$ denotes the largest integer less than or equal to x. The value of $\underline{m}$ is given by the condition $n_b(\underline{m}) = 1$.

It is possible to determine the global minimum of the energy $E(m, s_{0,+}(m))$ from the energy density of a squeelix of infinite length $e_{m<1}(m)$ (cf. Eq. (23)). The energy density $e_{m<1}(m)$ has a single minimum at $m = m^*$. Because of the cyclic nature of $\psi(s)$ a portion of length L_n of this infinite chain which contains, say $n - 1$ twist-kinks, must satisfy the relation

$$L_n = l_{cycle}(m^*)n - 2\Delta s(m^*) . \tag{40}$$

This value L_n is the length that allows to contain $n - 1$ twist-kinks in an optimal manner, *i.e.*, which minimizes $e_{m<1}(m)$. Here the twist angle reads $\psi(s) = am\left(\frac{s}{\lambda\sqrt{m^*}}\big|m^*\right)$ if n is even and $\psi(s) = am\left(\frac{s - l_{cycle}(m^*)/2}{\lambda\sqrt{m^*}}\big|m^*\right)$ if n is odd. But in both cases $\psi'(-L_n/2) = \psi'(L_n/2) = \omega_3$. In general the length L of the filament is given and is not equal to L_n. But if we choose n such that $L_n < L < L_{n+1}$, the state that minimizes the energy $E(m, s_{0,+}(m))$ is a state with $n_b = n$ or $n_b = n + 1$. The value of n can be found via Eq. (38) which gives $n_b(m^*)$. Then $n = \lfloor n_b(m^*)\rfloor$. Knowing n_b we determine m from Eq. (38).

4. Example

In this paragraph we consider an example to illustrate the theory. We show some shapes associated to the energy states (minima and maxima) of Fig. 6(a). The numbering of the shapes follows that of the figure: a shape designated
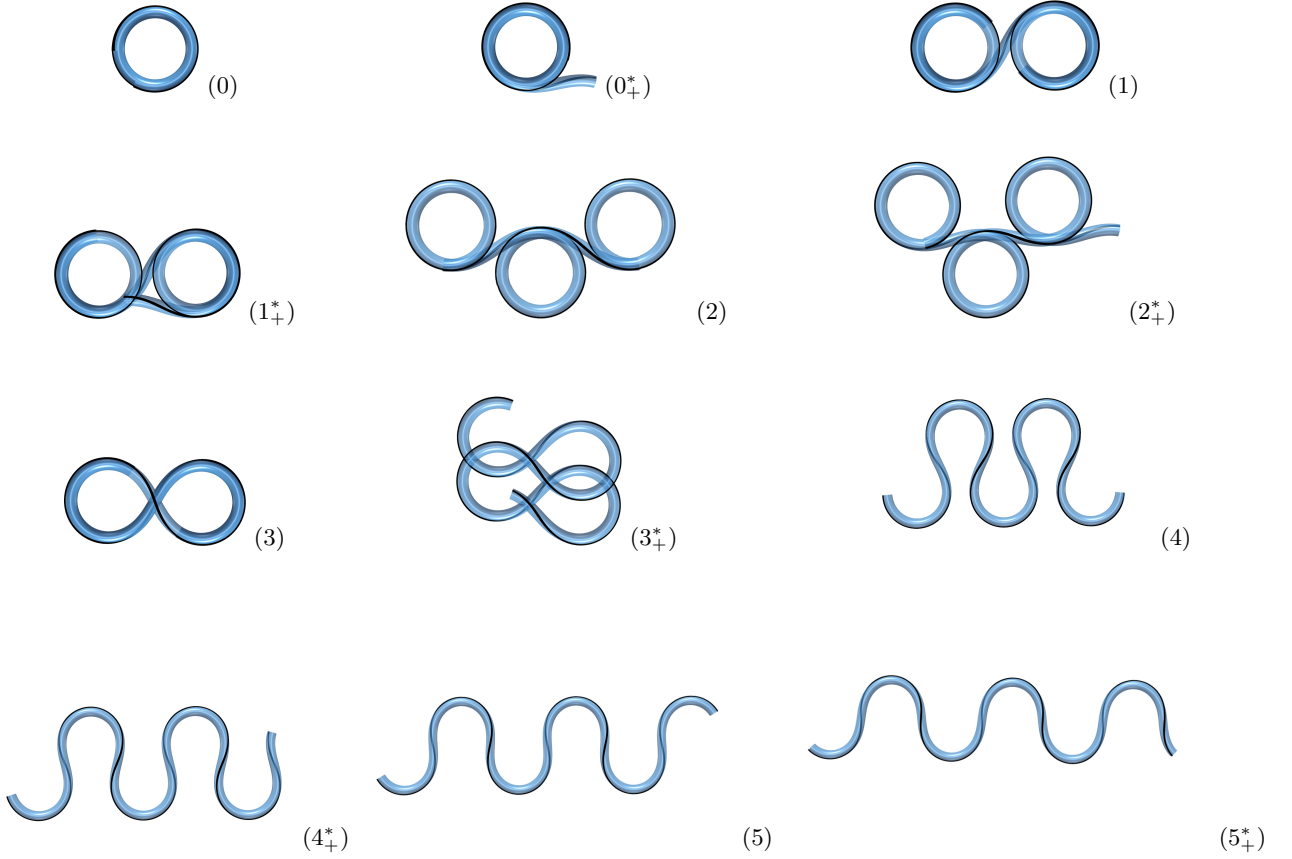
FIG. 7: Shapes of the squeelix in the regime $m < 1$ for $\gamma = 0.9915$.

FIG. 8: Examples of unstable shapes. The two shapes with a single critical twist-kink are labelled (0_+^*) and (0_-^*), and the shape with two critical twist-kinks (0_-^{**}).

by (n) has n twist-kinks and is a state of minimal energy, *i.e.*, $n_b = n+1$. A shape (n_+^*) is a critical shape (asymmetric and unstable) with $n_a = n+1$. It is the critical shape on the top of the energy barrier between the energy minima n and $n+1$. The symbol $+$ reminds us that we consider the line $s_{0,+}$. We measure all lengths in units of L and the energies in units of BL^{-1}. We also choose $\sqrt{C/B} = 1$. The shapes of the squeelix associated to the extrema of Fig. 6(a) and (b) will be very similar (because both energy curves are defined in a comparable range of m). Consequently, we will only consider the shapes associated to the extrema of the energy in Fig. 6(a), where $\gamma = 0.9915$, $\omega_1 = 24.4L^{-1}$ and $\omega_3 = 15.6L^{-1}$. In this case $0.7 \leq m \leq 2.44$ and the typical size of a twist-kink is $\lambda \approx 0.04L$ which allows a maximum number $n_{max} = 6$ of twist-kinks within the chain (from Eq. 39). We will treat the regions $m < 1$ and $m > 1$ separately.

   a.   Case $m < 1$.   Table I provides the values of $n_{a/b}$, m and the energies of the shapes shown in Fig. 7. The shape (0) consists of approximatively four circles on the top of each other (with deformed ends) as the perimeter of a single circle is $l_{loop} = 2\pi/\omega_1 \approx 0.26L$. The ground state is given by the shape (2) which has two twist-kinks, *i.e.*, $n_b = 3$. Squeelices of local energy minima (n) have symmetric shapes. Critical configurations (n^*) on the top of energy barriers are asymmetric with a critical twist-kink near the end $s = L/2$ of the filament.

   For completeness Fig. 8 shows three unstable shapes, in particular two critical shapes on the line $s_{0,-}(m)$. The shapes (0_-^*) and (0_+^*) have a critical twist-kink symmetrically localized at the opposite ends of their chain. They have the same energy $E_{0_+^*} = E_{0_-^*}$. The shape (0_-^{**}) has two critical twist-kinks localized at the two ends of the chain. Its energy is thus higher. Table II provides the numerical values of the parameters characterizing these shapes.

Shape	$n_{a/b}$	$m < 1$	Energy (BL^{-1})
(0)	$n_b = 1$	0.9999999999471	111.31
(0^*_+)	$n_a = 1$	0.999999999595	121.47
(1)	$n_b = 2$	0.99997091	111.11
(1^*_+)	$n_a = 2$	0.9999195	121.26
(2)	**$n_b=3$**	**0.997635**	**110.98**
(2^*_+)	$n_a = 3$	0.995359	121.23
(3)	$n_b = 4$	0.97955	111.72
(3^*_+)	$n_a = 4$	0.96651	122.56
(4)	$n_b = 5$	0.93093	115.18
(4^*_+)	$n_a = 5$	0.8990	127.71
(5)	$n_b = 6$	0.8563	123.36
(5^*_+)	$n_a = 6$	0.8043	139.00

TABLE I: Numerical values of the parameters of the shapes of Fig. 7. The ground state is written in bold face.

Shape	$n_{a/b}$	m	Energy (BL^{-1})
(0^*_+)	$n_a = 1$	0.999999999595	121.47
(0^*_-)	$n_a = 1$	0.999999999595	121.47
(0^{**}_-)	$n_b = 1$	0.9999999969	131.63

TABLE II: Numerical values of the parameters of the shapes of Fig. 8.

Shape	$n_{a/b}$	m	Energy (BL^{-1})
($\bar{1}$)	$n_b = 1$	1.000029	209.12
($\bar{1}^*_+$)	$n_a = 1$	1.00008	219.28
($\bar{2}$)	$n_b = 2$	1.0228	305.65
($\bar{2}^*_+$)	$n_a = 2$	1.0387	315.09

TABLE III: Numerical values of the parameters of the various shapes in Fig. 9.

  b. *Case $m > 1$.*   We consider the shapes of the squeelices associated to the four extrema in the region $m > 1$ of the energy in Fig. 6(a). Table III provides the numerical values of the parameters characterizing these shapes which are shown in Fig. 9. We observe that the shapes are similar to some of the shapes with $m < 1$ but have a higher energy. This is due to the presence of anti-twist-kinks which maximise the pure twist energy.

V.   HOW TO MEASURE THE MATERIAL PARAMETERS

  When confined biofilaments exhibit abnormal, wavy, spiral or circular shapes that cannot be explained by the semi-flexible chain model, the theory of squeelices developed here should be of some help. Assuming that the filament is in thermal equilibrium and does not display large thermal fluctuations, it is possible to have a quantitative understanding of the experimental biofilament under study, *i.e.*, a solid estimate of its material parameters.

  For a filament whose shape is wavy we know that $\gamma < 1$. The general procedure to obtain the material parameters
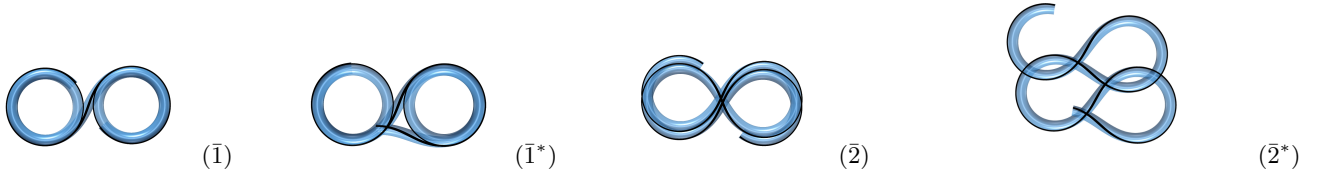

FIG. 9: Several shapes of the squeelix in the regime $m > 1$ for $\gamma = 0.9915$. The two shapes ($\bar{1}$) and ($\bar{2}$) minimize the energy of the squeelix. The shapes ($\bar{1}^*$) and ($\bar{2}^*$) have a single critical anti-twist-kink at one end of the chain and are unstable.

in this case consists of the following steps: (i) extract the tangent angle $\phi(s)$ from the experimental data and compute the curvature $\kappa(s)$. (ii) The maximum of $\kappa(s)$ gives ω_1. (iii) The length l_{cycle} corresponds to the distance between two adjacent roots of $\kappa(s)$. (iv) Via Eq. (22) one obtains λ in terms of m. (v) Plugging this result into the expression (16) of the curvature allows to fit the experimentally obtained curvature with a single parameter m. (vi) From m one obtains λ and thus the ratio C/B using Eq. (12). (vii) From Eq. (24) one finally gets γ from which ω_3 can be deduced.

A word of caution is due here. The suggested procedure neither takes into account excluded-volume interactions nor the effect of a finite temperature. Both can potentially modify the resulting shapes. Self-interactions are more important in the regime where the theoretical squeelix forms loops that lie on top of each other. In this case the repulsion will induce a separation of the circles. A strong self-interaction might even induce the formation of additional twist-kinks extending the filament and thus changing the ground state. In the regime $\gamma \ll 1$, where the shapes are wavy, self-interactions can be safely discarded.

In this article we have scaled all lengths with the length of the filament L. In these units the shape of a squeelix is scale invariant (the maximum number of twist-kinks in the chain, n_{max}, is independent of L) but its energy decreases with L (see, for instance, Tab. III). At zero temperature the theory can directly be applied to any microscopic or macroscopic system. For biofilaments at finite temperature, however, scale matters, and the natural energy scale is $k_B T$. The characteristic lengths of a biofilament (like λ) are fixed and independent of L and measured, for instance, in μm. The shape is not scale invariant any more. In these units the energy and n_{max} grow linearly with L (as one can see from Eq. (39) for n_{max}). At finite temperature the number of twist-kinks can fluctuate within the chain if the energy barrier ΔE between two adjacent minima with n and $n+1$ twist-kinks, respectively, of the energy $E(m, s_{0,+}(m))$ is of order $k_B T$. We can estimate this barrier from the energy contribution of the deformed ends (see text below Eq. (C1) in Appendix C): $\Delta E/k_B T \approx \frac{\omega_3^2}{\omega_1} \left(\frac{C}{B}\right)^{\frac{3}{2}} l_B$, where $l_B = B/k_B T$ is the persistence length associated to the bending of the filament. We expect strong shape fluctuations when $\Delta E/k_B T$ is of the order of one or smaller. Such strong fluctuations were already observed for a squeelix with circular ground state [19].

VI. CONCLUSION

A filament confined on a flat surface is frequently encountered in experiments to permit its observation in the focal plane. But generally, confinement modifies the elastic properties. This is particular blatant for filaments that adopt a helical shape in free space. The theory based on the linear elasticity of squeezed helical filaments is analogous to that of the two-dimensional Euler elastica. A lot of different shapes are found resembling circles, waves or spirals. Remarkably, a conformational quasi-particle called twist-kink emerges naturally from the model. In this picture the shapes of the squeelix result from the repulsive interaction of these quasi-particles. The extreme case of complete twist-kink expulsion from the chain could be the explanation for the formation of tiny actin rings confined to a flat surface [5]. In the same manner wavy and circular movements of microtubules in gliding assay experiments have been explained by the active movement of squeelices [26].

In this article we have elucidated the rich variety of shapes that can be found for these systems. This provides a nomenclature of squeezed helices that can potentially be usefull for the interpretation of experimental observations.

Confined elastic rods on a plane submitted to an additional lateral confinement were studied previously [27, 28]. An interesting extension of the present study would be to consider the case of squeelices under such a confinement. This seems particularly relevant in view of experiments with double confinement of biofilaments performed by Köster et al [29].

Appendix A: Euler-Lagrange equations of the squeelix

The elastic energy of the squeelix has been derived in the main text (see Eq. (6)):

$$E = \frac{1}{2} \int_{-L/2}^{L/2} \left[B\left(\phi' - \omega_1 \sin\psi\right)^2 + C\left(\psi' - \omega_3\right)^2 + B\omega_1^2 \cos^2\psi \right] ds \ . \tag{A1}$$
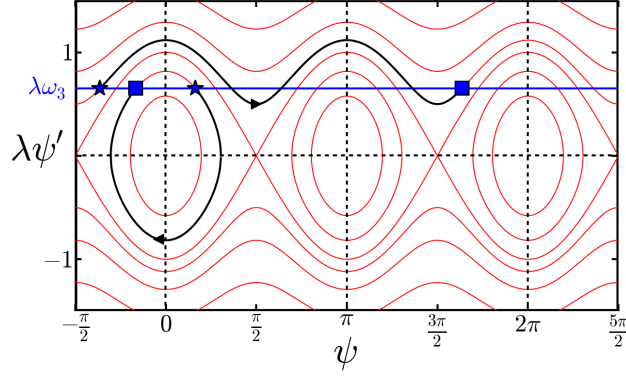
FIG. 10: Phase plane of Eq. (A7). Two typical trajectories are shown in black corresponding to the revolving ($m < 1$) and oscillating ($m < 1$) pendulum, which are solutions of Eq. (A6). The stars represent the position $s = -L/2$, the squares $s = L/2$. These points have to lie on the line $\lambda\omega_3$ due to the boundary conditions Eq. (A5).

Minimizing with respect to ϕ' gives

$$\phi' = \omega_1 \sin\psi \tag{A2}$$

and the energy becomes a function of $\psi(s)$:

$$E[\psi] = \frac{1}{2} \int_{-L/2}^{L/2} \left[C\left(\psi' - \omega_3\right)^2 + B\omega_1^2 \cos^2\psi \right] ds . \tag{A3}$$

The first variation of E with respect to ψ leads to

$$\delta E = -\int_{-L/2}^{L/2} ds \left(\left(C\frac{d}{ds}\left(\psi' - \omega_3\right) + \frac{1}{2}B\omega_1^2 \sin(2\psi) \right) \delta\psi \right) + \left[C\left(\psi' - \omega_3\right)\delta\psi \right]_{-L/2}^{L/2} \tag{A4}$$

with free boundary conditions, *i.e.*, no torque at both ends of the filament. The condition $\delta E = 0$ implies the Neumann boundary conditions:

$$\psi'(-L/2) = \psi'(L/2) = \omega_3 \tag{A5}$$

and the *pendulum* equation

$$\psi'' + \frac{1}{2\lambda^2}\sin(2\psi) = 0 \tag{A6}$$

with the length $\lambda = \frac{1}{\omega_1}\sqrt{\frac{C}{B}}$. Integrating Eq. ($A6$) we obtain $(\psi')^2 = a_1 - \frac{1}{2\lambda^2}\sin^2\psi$ with a_1 a positive constant of integration. This equation can be written conveniently in the following form

$$\psi'(s) = \pm\frac{1}{\lambda\sqrt{m}}\sqrt{1 - m\sin^2\psi} \tag{A7}$$

with $a_1 = 1/(\lambda^2 m)$ and m a positive real parameter.

The phase plane of Eq. (A7) is well-known and the solutions of Eq. (A6) are trajectories in this plane which begin and end at $\psi'(s) = \omega_3$ as shown in Fig. 10. Among all these trajectories the solutions we look for are those of length L. A similar approach with Dirichlet boundary conditions is considered in Ref. [30] for the determination of the equilibrium configurations of a uniform elastic rod subject to cantilever loading. The stability analysis of these solutions is discussed in Appendix E and their physical interpretation can be found in Appendix D. From Fig. 10 we see that when $\lambda\omega_3 > 1$ the solutions correspond to a revolving pendulum ($m < 1$) only. The oscillating pendulum ($m > 1$) is a solution only in the regime $\lambda\omega_3 < 1$.

Eq. ($A7$) implies $\psi(-L/2) = \pm\arcsin\sqrt{\frac{1}{m} - \frac{1}{\mu}} + n\pi$, with $n \in \mathbb{Z}$. Since $\phi' = \omega_1\sin\psi$ we can limit ourself to $n = 0$ and $n = 1$ without loss of generality. Since these two cases lead to two shapes related by the transformation

$\kappa(s) \to -\kappa(s)$ and thus have the same energy we treat the case $n = 0$ only. Consequently the twist angle at the first end can have one of the two values

$$\psi(-L/2) = \pm \arcsin \left(\sqrt{\frac{1}{m} - \frac{1}{\mu}} \right) . \tag{A8}$$

This implies that m lies in the interval

$$\frac{\mu}{1+\mu} \leq m \leq \mu \tag{A9}$$

with

$$\mu = \frac{B\omega_1^2}{C\omega_3^2} . \tag{A10}$$

As a consequence of Eq. $(A9)$ the twist is limited to the interval $-\pi/2 < \psi(-L/2) < \pi/2$. Integrating Eq. $(A7)$ with the positive sign

$$\int_{s_0}^{-\frac{L}{2}} ds = \lambda\sqrt{m} \int_0^{\psi(-\frac{L}{2})} \frac{d\psi}{\sqrt{1 - m\sin^2\psi}} \tag{A11}$$

yields s_0, given by the condition $\psi(s_0) = 0$, in terms of m for a given L:

$$s_0(m) = -\frac{L}{2} - \lambda\sqrt{m}\mathcal{F}(\psi(-L/2)|m) , \tag{A12}$$

where $\mathcal{F}(x|m)$ is the elliptic integral of the first kind, a growing function of x [23]. Eq. $(A12)$ defines two functions $s_{0,+}(m)$ and $s_{0,-}(m)$ depending on the sign of $\psi(-L/2)$. These two functions $s_{0,\pm}(m)$ are symmetric with respect to the line $s_0(m) = -L/2$, i.e., $s_{0,+}(m) = 2s_0(\mu) - s_{0,-}(m)$ and thus meet at the boundary $m = \mu$. Therefore $s_0(m)$ is defined in the interval

$$s_{0,-}(\frac{\mu}{1+\mu}) \leq s_0(m) \leq s_{0,+}(\frac{\mu}{1+\mu}) \tag{A13}$$

with $s_{0,\pm}(\frac{\mu}{1+\mu}) = -\frac{L}{2} \mp \lambda\frac{\pi}{2}\sqrt{\frac{\mu}{1+\mu}}$.

The explicit solution of Eq. (A6) is well-known:

$$\psi(s) = \pm am\left(\frac{s - s_0}{\lambda\sqrt{m}}\Big| m\right) , \tag{A14}$$

where $am(x|m)$ is the elliptic Jacobian amplitude function [23]. To obtain Eq. (A14) we have used the definition $\varphi = am(x|m)$ with $x = \int_0^\varphi \frac{d\theta}{\sqrt{1 - m\sin^2\theta}}$ and the relation $am(x|m) = -am(-x|m)$. As explained in the main text, the boundary condition $\psi'(-L/2) = \omega_3$ with $\omega_3 > 0$ imposes the positive sign in Eq. $(A7)$ in the vicinity of $-L/2$, so that we must choose

$$\psi(s) = am\left(\frac{s - s_0}{\lambda\sqrt{m}}\Big| m\right) . \tag{A15}$$

The twist $\psi(s)$ is a growing function of s for $m < 1$ and periodic for $m > 1$. The case $m = 1$ is the homoclinic pendulum with a single one-half turn, i.e., $\psi(s)$ changing by π on the length L.

The variation of the twist is given by

$$\psi'(s) = \frac{1}{\lambda\sqrt{m}} dn\left(\frac{s - s_0}{\lambda\sqrt{m}}\Big| m\right) , \tag{A16}$$

where $dn(x|m)$ is a periodic odd elliptic Jacobian function of period $l_p = 2\lambda\sqrt{m}\mathcal{K}(m)$ with $\mathcal{K}(m)$ the complete elliptic integral of the first kind [23]. The curvature $\kappa(s) = \phi'(s)$ given by Eq. $(A2)$ is then

$$\kappa(s) = \omega_1 sn\left(\frac{s - s_0}{\lambda\sqrt{m}}\Big| m\right) \tag{A17}$$

with $sn(x|m)$ a periodic even elliptic Jacobian function of period $l_p = 4\lambda\sqrt{m}\mathcal{K}(m)$ [23].

Appendix B: Energy of the squeelix

In this section we compute the elastic energy of a configuration given by Eq. (A15). From Eq. (A15) we have $\cos\psi = \text{cn}\left(\frac{s-s_0}{\lambda\sqrt{m}}|m\right)$. Plugging this expression together with ψ' from Eq. (A16) into the energy, Eq. (A3),

$$E = \frac{1}{2}\int_{-L/2}^{L/2}\left(B\omega_1^2\cos^2\psi + C\left(\psi'^2 - 2\omega_3\psi' + \omega_3^2\right)\right)ds , \tag{B1}$$

we see that we have to compute three integrals:

$$I_1 = \int_{-L/2}^{L/2}\text{cn}^2\left(\frac{s-s_0}{\lambda\sqrt{m}}|m\right)ds = \frac{\lambda}{\sqrt{m}}\left[\mathcal{E}\left(\frac{s-s_0}{\lambda\sqrt{m}}|m\right)\right]_{-L/2}^{L/2} + \left(1 - \frac{1}{m}\right)L , \tag{B2a}$$

$$I_2 = \int_{-L/2}^{L/2}\text{dn}^2\left(\frac{s-s_0}{\lambda\sqrt{m}}|m\right)ds = \lambda\sqrt{m}\left[\mathcal{E}\left(\frac{s-s_0}{\lambda\sqrt{m}}|m\right)\right]_{-L/2}^{L/2} , \tag{B2b}$$

$$I_3 = \int_{-L/2}^{L/2}\text{dn}\left(\frac{s-s_0}{\lambda\sqrt{m}}|m\right)ds = \lambda\sqrt{m}\left[\psi\left(s\right)\right]_{-L/2}^{L/2} , \tag{B2c}$$

where $\mathcal{E}\left(x|m\right)$ is the elliptic integral of the second kind [23]. To compute the integrals we have used $\int \text{cn}^2\left(s|m\right)ds = \frac{1}{m}\mathcal{E}\left(s|m\right) - \frac{(1-m)}{m}s$, $\int \text{dn}^2\left(s|m\right)ds = \mathcal{E}\left(s|m\right)$ and $\int \text{dn}\left(s|m\right)ds = \arcsin\left(\text{sn}\left(s|m\right)\right)$.

Consequently, we obtain the elastic energy

$$E = \frac{\omega_1\sqrt{BC}}{\sqrt{m}}\left(\mathcal{E}\left(\psi\left(L/2\right)|m\right) - \mathcal{E}\left(\psi\left(-L/2\right)|m\right)\right) + \frac{B\omega_1^2}{2}\left(1 + \frac{1}{\mu} - \frac{1}{m}\right)L - C\omega_3\left(\psi\left(L/2\right) - \psi\left(-L/2\right)\right)] . \tag{B3}$$

This expression is correct for all $m > 0$. However, when $m > 1$ it is advisable for numerical reasons to transform the Jacobi elliptic functions to their analogs with a parameter $1/m$ lower than unity. Using the relations $\text{cn}\left(s|m\right) = \text{dn}\left(\sqrt{m}s|\frac{1}{m}\right)$ and $\text{dn}\left(s|m\right) = \text{cn}\left(\sqrt{m}s|\frac{1}{m}\right)$ we obtain for the integrals

$$I_1 = \lambda\left[\mathcal{E}\left(\frac{s-s_0}{\lambda}|\frac{1}{m}\right)\right]_{-L/2}^{L/2} , \tag{B4a}$$

$$I_2 = \lambda m\left[\mathcal{E}\left(\frac{s-s_0}{\lambda}|\frac{1}{m}\right)\right]_{-L/2}^{L/2} + \left(1 - m\right)L , \tag{B4b}$$

$$I_3 = \lambda\left[\frac{\arccos\left(\text{dn}\left(\frac{s-s_0}{\lambda}|\frac{1}{m}\right)\right)\text{sn}\left(\frac{s-s_0}{\lambda}|\frac{1}{m}\right)}{\sqrt{1 - \text{dn}^2\left(\frac{s-s_0}{\lambda}|\frac{1}{m}\right)}}\right]_{-L/2}^{L/2} . \tag{B4c}$$

Therefore, the energy formula (B3) can also be conveniently written

$$E_{m>1} = \omega_1\sqrt{BC}\left[\mathcal{E}\left(\frac{s-s_0}{\lambda}|\frac{1}{m}\right)\right]_{-L/2}^{L/2} + \frac{B\omega_1^2}{2}\left(-1 + \frac{1}{\mu} + \frac{1}{m}\right)L - C\omega_3\left[\frac{\arccos\left(\text{dn}\left(\frac{s-s_0}{\lambda}|\frac{1}{m}\right)\right)\text{sn}\left(\frac{s-s_0}{\lambda}|\frac{1}{m}\right)}{\sqrt{1 - \text{dn}^2\left(\frac{s-s_0}{\lambda}|\frac{1}{m}\right)}}\right]_{-L/2}^{L/2}$$
$$\tag{B5}$$

for $m > 1$.

Consider the elastic energy, Eq. (B3), as a function of m and s_0. The domain of admissible values for the variables is defined by Eqs. (A9) and (A13). Fig. 11 shows an example: One observes a complex energy landscape with a lot of extrema, that are minima, maxima and saddle points. These extrema correspond to the stable or unstable shapes of the squeelices verifying the boundary conditions Eqs. (A5). The function $E(m, s_0(m))$ where $s_0(m)$ is given by Eq. (A12) represents a trajectory on the energy landscape $E(m, s_0)$ that passes by all its extrema. We also observe a sharp distinction in the behavior of the $E(m, s_0)$ for the revolving $(m < 1)$ and oscillating pendulum $(m > 1)$, respectively (see Fig. 11). In the main text, we discuss the shapes of the squeelices that are associated to all these extrema.
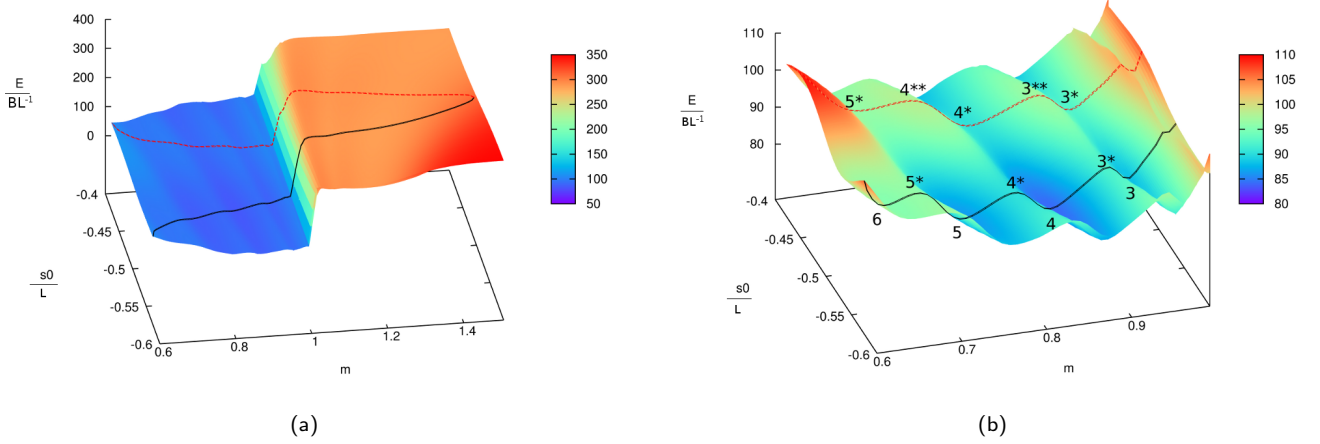
FIG. 11: Energy landscape $E(m, s_0)$ for $\gamma = 0.6079$, $\omega_1 = 20L^{-1}$, $\omega_3 = 16.33L^{-1}$ and $\sqrt{C/B} = 1$. Energies and lengths are measured in units of BL^{-1} and L, respectively. (a) The curve $s_{0,+}(m)$ in black passes by all minima and the curve $s_{0,-}(m)$ in red passes by all maxima. Both curves also pass by saddle points of same energy. (b) Zoom of the energy in the regime $m < 1$. The integers n, n^* and n^{**} denote the minima, the saddle points and the maxima, respectively.

Appendix C: Life without Jacobi elliptic functions—the twist-kink picture

The concept of a twist-kink was introduced in Ref. [19] by an analogy between the energy of the squeelix and the energy of a semi-flexible chain under tension which contains sliding loops [31, 32]. We will not use this analogy here. Instead we will exploit the results of Appendix A to determine the shape of a single twist-kink. In this maybe more physical approach we will not need Jacobi elliptic functions for the description of the shapes. The drawback is that we are limited to the regimes $m \approx 1$ and $m \approx 0$ as we will see in the following.

Neglecting the boundary conditions Eq. ($A5$) one directly obtains the trivial solution $\psi(s) \approx \pm\pi/2$. The shape is circular with constant radius of curvature $1/\omega_1$ and energy $E_0 = C\omega_3^2 L/2$. For a squeelix of finite length L, the boundary conditions Eq. ($A5$) impose deformations at both ends of the chain. For small deformations $\psi(s) \pm \pi/2 \ll 1$ at the chain's ends, and the solution can be written approximately as [19]

$$\psi(s) \approx \frac{\lambda\omega_3 \sinh(s/\lambda)}{\cosh(L/(2\lambda))} \pm \pi/2 \ , \tag{C1}$$

which is valid in the regime $\lambda\omega_3 \ll 1$. The energy of this configuration is $\widetilde{E}_0 \approx (2\lambda/L + 1)E_0$. Thus, $2\lambda E_0/L$ is the energy contribution of the deformed ends. Note that for large deformations at the boundary, the exact solution Eq. ($A15$) must be considered because deformations at the ends are actually pieces of a twist-kink. This case is treated in Appendix D. For now we assume that $\lambda\omega_3/L \ll 1/L$.

We now consider a twist angle $\psi(s)$ that increases by π along the chain. The solution is given by Eq. ($A15$) with $m = 1$ and reads

$$\psi(s) = 2\arctan(e^{s/\lambda}) - \pi/2 \tag{C2}$$

with $\psi(-\infty) = -\pi/2$ and $\psi(\infty) = \pi/2$. The curvature is thus

$$\phi' = \omega_1 \tan(s/\lambda) \ . \tag{C3}$$

For $\lambda/L \ll 1$ the shape is made of two circular arcs of inverse curvature separated by a region of curvature inversion of size λ that we have named a twist-kink [19]. The energy of this configuration is

$$E_{1TK} = \pi C\omega_3 (\gamma - 1) + \frac{C\omega_3^2}{2}L \tag{C4}$$

with $\gamma = \frac{4\omega_1^2 B}{\pi^2 \omega_3^2 C}$. We could take into account the effect of the boundary conditions by simply adding their elastic energy $\approx 2\lambda E_0/L$ to E_{1TK}. Comparing with the zero twist-kink case $E_0 = C\omega_3^2 L/2$ we find an expression for the

self-energy of a twist-kink:

$$\Delta E_1 = E_{1TK} - E_0 = \pi C \omega_3 \left(\sqrt{\gamma} - 1 \right) . \tag{C5}$$

Therefore, $\gamma = 1$ separates the regimes of positive and negative self-energy. For $\gamma > 1$ the ground state is a circular arc. Decreasing γ, twist-kinks will pop-up within the chain with a density limited by their mutual repulsion. This corresponds to the regime $m \lesssim 1$ (the revolving pendulum). To give a more quantitative foundation to this argument let us compute the interaction energy of two twist-kinks separated by a distance d such that $d/\lambda \gg 1$. In this dilute regime $\gamma \lesssim 1$.

With the following two twist-kinks ansatz

$$\psi(s) = 2 \arctan \left(e^{(s+d/2)/\lambda} \right) + 2 \arctan \left(e^{(s-d/2)/\lambda} \right) - \frac{\pi}{2} , \tag{C6}$$

such that $\psi(-\infty) = -\pi/2$ and $\psi(\infty) = 3\pi/2$, the energy reads

$$E_{2TK} - E_0 = 2\Delta E_1 + 4\sqrt{CB}\omega_1 \exp(-d/\lambda)) . \tag{C7}$$

The repulsive interaction between two twist-kinks scales as $\sim \exp(-d/\lambda)$ in the dilute regime $\lambda \ll d$. Generalizing for n twist-kinks, with a mutual separation $d = L/(n+1) \gg \lambda$ we obtain the relation

$$E_{nTK}^{dilute} - E_0 \approx n\Delta E_1 + 2n\sqrt{CB}\omega_1 \exp(-\frac{L}{\lambda(n+1)}) . \tag{C8}$$

For $n \gg 1$ the optimal value n^* will correspond to the largest integer such that $E_{nTK}^{dilute} - E_{(n-1)TK}^{dilute} < 0$, which leads to

$$n^* = \left\lfloor \frac{L}{\lambda \ln \left(\sqrt{\gamma}/ \left(1 - \sqrt{\gamma} \right) \right)} \right\rfloor , \tag{C9}$$

where $\lfloor x \rfloor$ is the notation for the largest integer less than or equal to x. For $\gamma \lesssim 1$, the density $\rho = n^*/L$ is very small and the shapes consist of a succession of circular arcs (or spirals) with opposite curvatures and separated by twist-kinks (see figures in the main text). It is interesting to compare this density with the exact density $\rho = 1/l_{cycle} = (2\lambda\sqrt{m}K(m))^{-1}$ which is approximately $(\lambda \ln(\frac{16}{1-m}))^{-1}$ for $m \lesssim 1$. Comparing the two expressions of the density we find the relation $m \approx 17 - 16/\sqrt{\gamma}$ between m and γ.

Note that the oscillating pendulum ($m > 1$) can be treated similarly in this dilute regime. But now Eq. ($C7$) must be interpreted in terms of the mutual repulsion between twist-kinks and anti-twist-kinks. Corresponding shapes are thus similar to the revolving pendulum case. However, in the regions where the curvature changes sign, ψ goes to zero instead of repeatedly increasing by π. In the main text it is shown that the oscillating pendulum is never the ground state of the squeelix. This is easy to understand. An oscillating twist ψ implies that its derivative $\psi'(s)$ changes sign periodically. A negative derivative increases the pure twist energy around the curvature inversion point by $\frac{C}{2} \int (\psi' - \omega_3)^2 ds \sim \lambda C \omega_3^2/2 = \lambda E_0/L$. Nevertheless, this contribution is small for $\lambda/L \ll 1$.

The right-hand side of Eq. (C9) diverges as $\sqrt{\gamma}$ approaches $1/2$, which would mean that one can pack an arbitrary large number of TKs in a chain of length L. This divergence is non-physical and is due to the fact that the long-range repulsive interaction $e^{-d/\lambda}$ is not strong enough to stabilize the gas of twist-kinks against collapsing. Therefore, we must look at the opposite regime of high twist-kink density and compute the short-range repulsion between them.

When $\gamma \approx 0$ is decreased, the twist-kinks get more confined and their density becomes high. They are also very deformed compared to their free state Eq. ($C2$) and the notion of individual twist-kinks actually looses its meaning. Nevertheless, we keep using the terminology for convenience. When the separation between adjacent twist-kinks is $d \ll \lambda$, the chain is being forced to overtwist so that $\psi(s)$ tends to become linear with s. A good ansatz in this regime is

$$\psi(s) = \frac{\pi}{d}s - \frac{\pi}{2} \quad \text{for } 0 \ll s \ll L = nd , \tag{C10}$$

where n the number of twist-kinks along the chain (as $\psi(L) - \psi(0) = \pi n$) is assumed very large. In this regime $m \approx 0$. The curvature becomes

$$\kappa(s) \approx \omega_1 \cos \frac{\pi}{d}s . \tag{C11}$$

λ/d	E_{nTK}^{dense}	E_{nTK}^{dilute}	E
10^2	1600.	-3.10^8	1580.
10	1600.	-2.10^6	1580.
1	1600.	-1.10^4	1570.
10^{-1}	1600.	962.	954.
3.10^{-2}	1600.	370.	369.

TABLE IV: Comparison of the energies in the twist-kink picture with the exact result. The values are obtained with $\omega_1 = \omega_3 = 80L^{-1}$, $n = 26$, and $\lambda\omega_3 \approx 0.3$. All energies are given in units of B/L.

Pluging Eq. ($C10$) in Eq. (A1) the total energy in this dense regime is

$$E_{nTK}^{dense} \approx \frac{\omega_1^2 B}{4} L + \frac{\pi^2}{2} \frac{C n^2}{L} - \pi C \omega_3 n + E_0 \;, \tag{C12}$$

so that the optimum number n^* minimizing this energy is

$$n^* \approx \frac{\omega_3}{\pi} L \;. \tag{C13}$$

Therefore, $\psi(s) = \omega_3 s$ and $\psi'(s) = \omega_3$ which satisfies the boundary conditions automatically. The tangent angle to the filament is then given by

$$\phi(s) = \phi(-L/2) + \omega_1 \sin(\omega_3 s) \;. \tag{C14}$$

Note that in the case of the oscillating pendulum, when $\gamma \approx 0$, the twist-kink-anti-twist-kink couple is very dense and the energetic cost of the twist contribution is very high when $\psi(s)$ oscillates very fast. Therefore, it is not necessary to treat this case further.

Taking a large value of n and varying λ one obtains Table IV which shows a quantitative comparison between the energies in the twist-kink picture and the exact expression, Eq. (B3). We observe a good agreement in both asymptotic regimes $\lambda/d \ll 1$ and $\lambda/d \gg 1$.

The approach of this section can be used to explain the different shapes discussed in the main text in a physical manner. In particular, it is valid in the regime of very low and very high density of twist-kinks for the case of infinite long chains, but also for finite chains as long as the boundary effects can be neglected.

Appendix D: Squeelices of finite length

In this section we will treat the problem exactly. We will nevertheless refer to the twist-kink nomenclature whenever it is convenient. We will consider the cases of the revolving and the oscillating pendulum separately.

1. The revolving pendulum ($m < 1$)

In this regime the twist, given by Eq. (A15), is a growing function of s. Eq. (A7) reads with the positive sign

$$\psi'(s) = \frac{1}{\lambda\sqrt{m}}\sqrt{1 - m\sin^2\psi} = \frac{1}{\lambda\sqrt{m}} dn\left(\frac{s - s_0}{\lambda\sqrt{m}}\Big|m\right) > 0 \;, \tag{D1}$$

where $dn(x|m)$ is a periodic odd elliptic Jacobian function of period $l_p = 2\lambda\sqrt{m}K(m)$ which is positive in this regime, i.e., $1 \le dn(x|m) \le \sqrt{1-m}$ [23]. The boundary conditions $\psi'(-L/2) = \psi'(L/2) = \omega_3$ imply

$$\sin\psi(-L/2) = \pm\sin\psi(L/2) \;, \tag{D2}$$

which is equivalent to the two cases

$$\psi(L/2) = \psi(-L/2) + n_a\pi \quad \text{(case (a))} \qquad \text{and} \tag{D3a}$$
$$\psi(L/2) = -\psi(-L/2) + n_b\pi \quad \text{(case (b))} \;, \tag{D3b}$$

where $n_a, n_b \in \mathbb{Z}$. In both cases $\psi(-L/2)$ equals $\pm\arcsin\left(\sqrt{\frac{1}{m} - \frac{1}{\mu}}\right)$ according to Eq. (A8). This leads to four typical trajectories in the phase plane (see Fig. 12). Our goal is to identify those trajectories that satisfy the length constraint, i.e., to find all possible values of m for a given L.
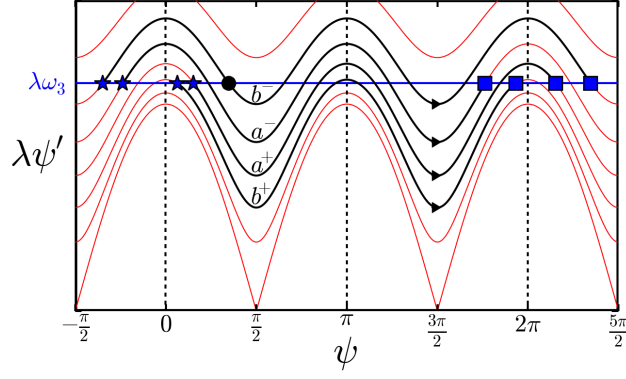
FIG. 12: Phase plane of the revolving pendulum with four typical trajectories in black associated to the cases (a) and (b) (see Eqs. (D3)). The stars represent the position $s = -L/2$, the squares $s = L/2$ for these trajectories. The subscript $\pm$ refers to the sign of $\psi(-L/2)$, which is either positive or negative. The shown trajectories correspond to shapes with a single twist-kink in the bulk of the chain, i.e., $n_a = n_b = 2$. They are shown for illustrative reasons but do not have the same length. Nevertheless, with this restriction in mind we see that a^+ has a shape of type (1^*_+), a^- of type (1^*_-), b^- of type (1^{**}), and b^+ of type (1) as depicted in Fig. 15. In Appendix E we show that only the trajectories of type b^+ lead to stable shapes. The black circle indicates the position $s = L/2$ of the case $n_b = 0$ (see text).

Case (a)

An illustration of this case is given by the trajectories a^+ and a^- in Fig. 12. Using the relation $am\,(x|m) + k\pi = am\,(x + 2k\mathcal{K}(m)|m)$, Eq. $(D3a)$ leads to

$$L = 2n_a\lambda\sqrt{m}\mathcal{K}(m) \tag{D4}$$

with $n_a = +1, +2,...$ Here n_a is the number of curvature inversion points within the filament (when $\psi = k\pi$ with k a natural number). For each allowed value of n_a there is a single solution of Eq. (D4) with a particular m.

Since m lies in the interval $\frac{\mu}{1+\mu} \leq m \leq \mu$ for $\mu < 1$ and $\frac{\mu}{1+\mu} \leq m \leq 1$ for $\mu \geq 1$ the length L is bounded by

$$L_{\min} \leq \frac{L}{n_a} \leq L_{\max} \tag{D5}$$

with $L_{\min} = 2\lambda\sqrt{\frac{\mu}{1+\mu}}\mathcal{K}(\frac{\mu}{1+\mu})$ and $L_{\max} = 2\lambda\sqrt{\mu}\mathcal{K}(\mu)$ for $\mu < 1$ or $L_{\max} \to \infty$ for $\mu \geq 1$.

In order to satisfy the condition of acceptable values of L, Eq. $(D5)$, the number of twist-kinks is limited, i.e., $n_a \in [n_{a,\min}, n_{a,\max}]$ with $n_{a,\min} = \lfloor L/L_{\max} \rfloor$ and $n_{a,\max} = \lfloor L/L_{\min} \rfloor$. The notation $\lfloor x \rfloor$ again denotes the largest integer less than or equal to x.

For $n_a = 1$, the chain contains a curvature inversion point or a *single* partial twist-kink which is localized close to one end of the chain. This requires a minimum length $L_{\min}$.

From Eq. $(A12)$ we obtain:

$$s_{0,\pm} = -\frac{L}{2} \mp \lambda\sqrt{m}\mathcal{F}\left(\arcsin\left(\sqrt{\frac{1}{m} - \frac{1}{\mu}}\right) \Big| m\right) . \tag{D6}$$

We have thus two different solutions $\psi(s)$ and consequently two different shapes of the squeelix. The stability analysis of Appendix E shows that all these shapes are *unstable*, i.e., saddle points of the elastic energy $E[\psi]$ (see Eq. (A3)) of the squeelix.

For $s_{0,+}$ the shape has $n_a - 1$ twist-kinks in the bulk and a curvature inversion point, called critical twist-kink, near $s = L/2$. These shapes are the maxima of the curve $E(m, s_{0,+}(m))$. The case $s_{0,-}$ is very similar except that the critical twist-kink is situated near $s = -L/2$. Although they are minima of $E(m, s_{0,-}(m))$ they have the same energy than their $s_{0,+}$ counterpart. These two shapes labelled (n^*) in Figs. 13 and 14 are saddle points of the energy landscape $E(m, s_0)$ with the same energy. They are the critical shapes on the top of the energy barrier of $E(m, s_{0,+}(m))$ that must be overcome to inject or expel a single critical twist-kink (localized at one of the ends of the squeelix) within the chain (see Fig. 14).
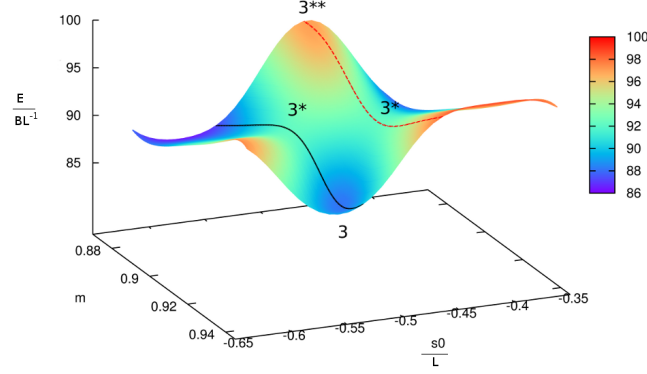
FIG. 13: Zoom of the energy landscape $E(m, s_0)$ for $\gamma = 0.6079$, $\omega_1 = 20L^{-1}$, $\omega_3 = 16.33L^{-1}$ and $\sqrt{C/B} = 1$. The curve $s_{0,+}(m)$ passes by the minimum 3 (containing three twist-kinks, *i.e.*, n_b=4), then the saddle point 3* (n_a=4) and goes to the next minimum 4 (with n_b=5, not shown). The curve $s_{0,-}(m)$ comes from the maximum 2** (n_b=3, not shown), then passes by the saddle point 3* and reaches the next maximum 3** (n_b=4). Energies and lengths are measured in units of BL^{-1} and L, respectively.
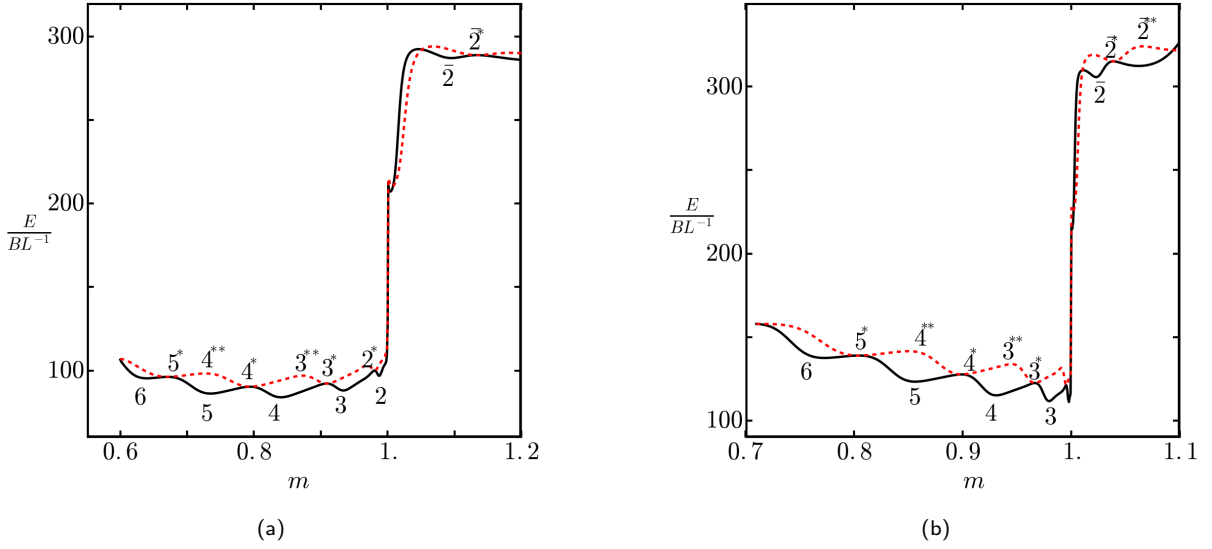

(a)

(b)

FIG. 14: The energies $E(m, s_{0,+}(m))$ (black solid curve) and $E(m, s_{0,-}(m))$ (red dotted curve), respectively for (a) $\gamma = 0.6079$, $\omega_1 = 20L^{-1}$, $\omega_3 = 16.33L^{-1}$ and $\sqrt{C/B} = 1$. (b) $\gamma = 0.9915$, $\omega_1 = 24.4L^{-1}$, $\omega_3 = 15.6L^{-1}$ and $\sqrt{C/B} = 1$. The case (b) is discussed in detail in the main text. Energies and lengths are measured in units of BL^{-1} and L, respectively.

Case (b)

An illustration of this case is given by the trajectories b^+ and b^- in Fig. 12. Using the properties $am\,(x|m) + k\pi = am\,(x + 2k\mathcal{K}(m)|m)$ and $am\,(x|m) = -am\,(-x|m)$ Eq. (D3b) implies

$$s_0 = -n_b\lambda\sqrt{m}\mathcal{K}(m)\,. \tag{D7}$$

Plugging this result into Eq. (A12) we obtain:

$$L = 2\lambda\sqrt{m}\left[n_b\mathcal{K}(m) \mp \mathcal{F}\left(\arcsin\sqrt{\frac{1}{m} - \frac{1}{\mu}}\Big|m\right)\right]\,. \tag{D8}$$

Thus for each value of n_b, we have two values for m that satisfy Eq. (D8) and thus two values $s_{0,\pm}$. The two associated shapes are very different as explained in the main text.

(i) The case with the plus sign in Eq. (D8) corresponds to the initial condition $\psi(-L/2) = -\arcsin\left(\sqrt{\frac{1}{m} - \frac{1}{\mu}}\right)$, *i.e.*, the trajectory $s_{0,-}$. In Appendix E it is shown that all these extrema on the trajectory $s_{0,-}$ are *unstable*.

Consider first $n_b = 0$ which corresponds to the portion of trajectory of b^- between the star and the circle in Fig. 12. The ψ is an incomplete twist-kink centered in the middle of the chain, *i.e.*, $s_0 = 0$. One can show that this symmetric solution is a minimum of the curve $E(m, s_{0,-}(m))$ but a saddle point of the landscape $E(m, s_0)$. It turns out that this solution does not exist for $L > L_{min}$.

For $n_b = 1, 2...$ similar to case (a) the length L is bounded by

$$(n_b + 1) L_{\min} \leq L \leq n_b L_{\max} \tag{D9}$$

In order to satisfy the condition above, $n_b \in [n_{b,\min}, n_{b,\max}]$ with $n_{b,\min} = \lfloor L/L_{\max} \rfloor$ and $n_{b,\max} = \lfloor L/L_{\min} \rfloor - 1$. Note that for $n_b = 1$ there is a minimum length, *i.e.*, $2L_{\min} \leq L \leq L_{\max}$. The reason for this is that there are *two* critical twist-kinks within the chain for $n_b = 1$, localized at both ends (see Fig. 15).

These symmetric solutions, labelled (n^{**}), are maxima of the curve $E(m, s_{0,-}(m))$ and maxima of the landscape $E(m, s_0)$. They are the critical shapes with two critical twist-kinks (localized at both ends of the squeelix) on the top of the energy barrier of $E(m, s_{0,-}(m))$ that must be overcome to inject or expel one or both twist-kinks (see Figs. 13 and 14).

(ii) The case with the minus sign in Eq. $(D8)$ corresponds to the initial condition $\psi(-L/2) = \arcsin\left(\sqrt{\frac{1}{m} - \frac{1}{\mu}}\right)$, *i.e.*, the trajectory $s_{0,+}$. In this case one obtains

$$(n_b - 1) L_{\min} \leq L \leq n_b L_{\max} \tag{D10}$$

with $n_b = 1, 2...$ In order to satisfy this condition $n_b \in [n_{b,\min}, n_{b,\max}]$ with $n_{b,\min} = \lfloor L/L_{\max} \rfloor$ and $n_{b,\max} = 1 + \lfloor L/L_{\min} \rfloor$. Note that for $n_b = 1$ the length L can be arbitrarily small, *i.e.*, $0 < L \leq L_{\max}$. This is the situation with *zero* twist-kinks within the chain. It is thus the ground state for $\gamma > 1$ and corresponds to Eq. $(C1)$. When $L > L_{\min}$, a twist-kink can be injected within the chain. It will be localized in the center of the squeelix. More twist-kinks will be disposed in an equidistant manner (see Fig. 15). Here $n_b - 1$ gives the number of twist-kinks in the squeelix. These solutions are local minima of the energy $E(m, s_{0,+}(m))$ (see Figs. 13 and 14). As shown in the stability analysis of Appendix E, these solutions lead to *stable shapes* that are also minima of the full elastic energy $E[\psi]$ of the squeelix.

Note that the case $m = 1$ gives

$$\psi(s) = 2\arctan\left(\frac{s - s_{0,+}(1)}{\lambda}\right) - \pi/2 \tag{D11}$$

with $s_{0,+}(1)$ given by Eq. (D6). This function satisfies the boundary condition at $s = -L/2$ by construction but $\psi'(L/2) < \omega_3$. Therefore, it is never a solution of the equation of motion of a squeelix of finite length.

Figure 15 illustrates the theory developped in this appendix. It shows the shapes that are associated to the first extrema in Fig. 14(b) in the regime $m < 1$. For further shapes of this example with $m < 1$ see Fig. 7 in the main text.

2. The oscillating pendulum $(1 < m)$

For $m > 1$ the twist, Eq. $(A15)$, is a periodic function of period $l_p = 4\lambda\mathcal{K}(\frac{1}{m})$. We used the fact that $\mathcal{K}(m) = \frac{1}{\sqrt{m}}\mathcal{K}(\frac{1}{m})$ for $m > 1$. The amplitude of the oscillations is $\psi_0 = \arcsin\sqrt{1/m} < \pi/2$. The twist variation Eq. $(A7)$ is then very different from its $m < 1$ counterpart

$$\psi'(s) = \frac{1}{\lambda\sqrt{m}} cn\left(\frac{s - s_0}{\lambda} \Big| \frac{1}{m}\right), \tag{D12}$$

where $cn(x|m)$ is an odd periodic elliptic Jacobian function that oscillates between -1 and 1 and thus changes its sign [23]. In this regime the periodic curvature reads

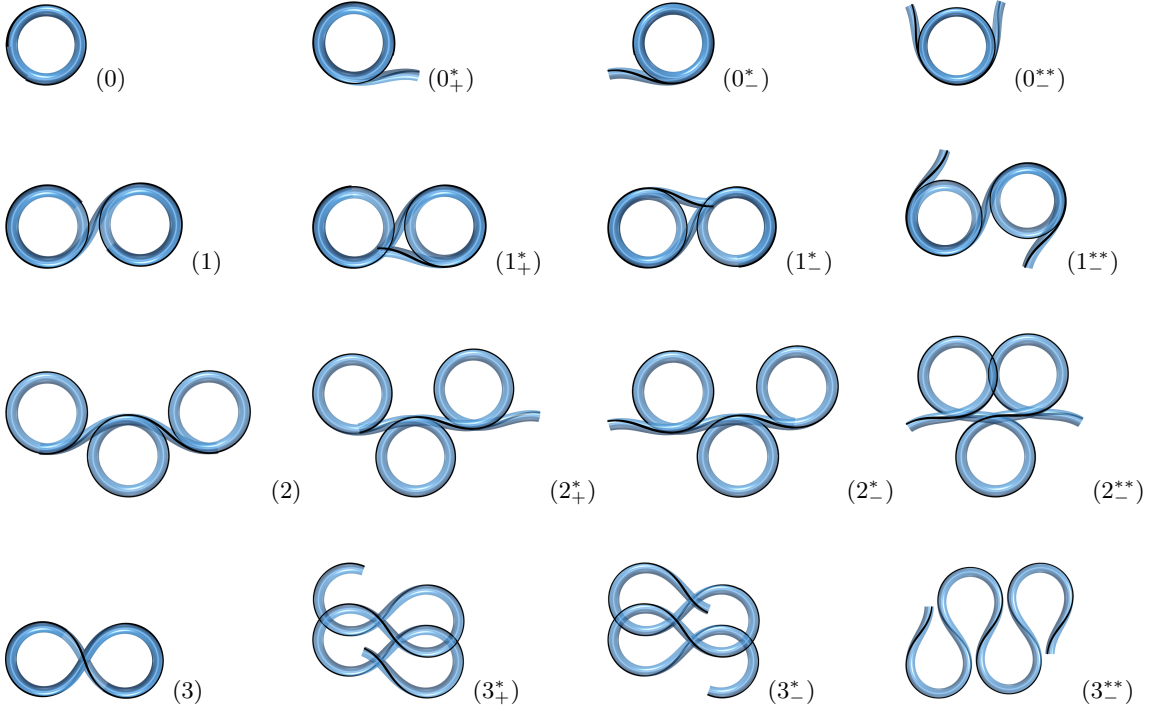$$\kappa(s) = \frac{\omega_1}{\sqrt{m}} sn\left(\frac{s - s_0}{\lambda} \Big| \frac{1}{m}\right) \tag{D13}$$

FIG. 15: Shapes of the squeelix in the regime $m < 1$ for $\gamma = 0.9915$, $\omega_1 = 24.4L^{-1}$, $\omega_3 = 15.6L^{-1}$ and $\sqrt{C/B} = 1$. These shapes correspond to the first extrema of the energy in Fig. 14(b).

Shape	$n_{a/b}$	m	Energy (BL^{-1})
(0)	$n_b = 1$	0.9999999999471	111.31
(0^*_+)	$n_a = 1$	0.999999999595	121.47
(0^*_-)	$n_a = 1$	0.999999999595	121.47
(0^{**}_-)	$n_b = 1$	0.9999999969	131.63
(1)	$n_b = 2$	0.99997091	111.11
(1^*_+)	$n_a = 2$	0.9999195	121.26
(1^*_-)	$n_a = 2$	0.9999195	121.26
(1^{**}_-)	$n_b = 2$	0.9997774	131.42
(2)	**$n_b=3$**	**0.997635**	**110.98**
(2^*_+)	$n_a = 3$	0.995359	121.23
(2^*_-)	$n_a = 3$	0.995359	121.23
(2^{**}_-)	$n_b = 3$	0.99089	131.54
(3)	$n_b = 4$	0.97955	111.72
(3^*_+)	$n_a = 4$	0.96651	122.56
(3^*_-)	$n_a = 4$	0.96651	122.56
(3^{**}_-)	$n_b = 4$	0.94501	133.87

TABLE V: Numerical values of the parameters of the shapes of Fig. 15.

with the period l_p. The boundary condition $\psi'(-L/2) = \psi'(L/2) = \omega_3$ now implies the following cases

$$\psi(L/2) = \psi(-L/2) \quad \text{(case (a))} , \tag{D14a}$$
$$\psi(L/2) = -\psi(-L/2) \quad \text{(case (b))} , \tag{D14b}$$

which corresponds to equal (a) or opposite (b) curvatures at the ends of the squeelix. Eq. $(A8)$ is still valid, *i.e.*, $\psi(-L/2) = \pm \arcsin\left(\sqrt{\frac{1}{m} - \frac{1}{\mu}}\right)$. Thus $-\psi_0 \leq \psi(-L/2) \leq \psi_0$ which implies $1 \leq m \leq \mu$. The equation for s_0
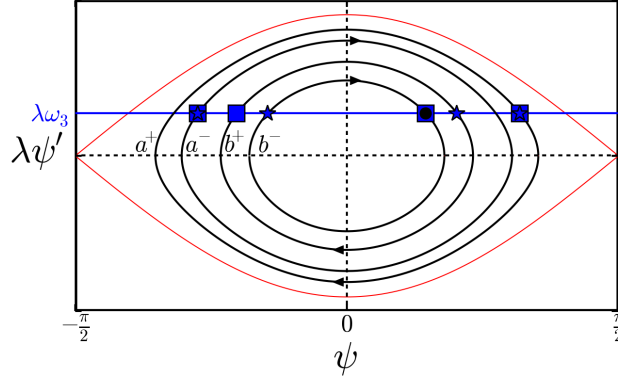
FIG. 16: Phase plane of the oscillating pendulum with four typical trajectories in black associated to the cases (a) and (b) (see Eqs. (D14)). The stars represent the position $s = -L/2$, the squares $s = L/2$ for these trajectories. The subscript $\pm$ refers to the sign of $\psi(-L/2)$, which is either positive or negative. In Appendix E we show that only the trajectories of type b^+ lead to stable shapes. The black circle indicates the position $s = L/2$ of the case $n_b = 0$ (see text).

becomes

$$s_{0,\pm} = -\frac{L}{2} \mp \lambda \mathcal{F}\left(\arcsin\left(\sqrt{1 - \frac{m}{\mu}}\right) | \frac{1}{m}\right) , \tag{D15}$$

where $s_{0,+}$ corresponds to $0 < \psi(-L/2) < \pi/2$ and $s_{0,-}$ to $-\pi/2 < \psi(-L/2) < 0$. We used the relation $\mathcal{F}(\varphi|m) = \frac{1}{\sqrt{m}}\mathcal{F}\left(\arcsin(\sqrt{m}\sin\varphi)|\frac{1}{m}\right)$.

Case (a)

An illustration of this case is given by the trajectories a^+ and a^- in Fig. 16. Eq. $(D14a)$ implies

$$L = n_a l_p(m) , \tag{D16}$$

where $n_a = +1, +2, \ldots$ is the number of periods in the chain. We have the constraint

$$l_p(\mu) \leq \frac{L}{n_a} \tag{D17}$$

as $K\left(\frac{1}{m}\right) \to \infty$ with $m \to 1$. Therefore $1 \leq n_a \leq n_{a,\max}$ with $n_{a,\max} = \lfloor L/l_p(\mu) \rfloor$. For a given length there is a maximal number of oscillations. For each allowed value of n_a there is one solution of Eq. $(D16)$ with a given m. The arc length s_0 is related to L by Eq. $(D15)$.

The associated shapes turn out to be *unstable* (see Appendix E). The two types of shapes obtained with $s_{0,\pm}$ have the same energy. They correspond to the critical shapes on the top of the energy barrier that must be overcome to inject or expel a single anti-twist-kink (localized at the chain end $s = L/2$ for $s_{0,+}$ or at $s = -L/2$ for $s_{0,-}$) within the chain (see main text for some shapes).

Case (b)

An illustration of this case is given by the trajectories b^+ and b^- in Fig. 16. Equation (D14b) implies $am\left(\frac{L/2-s_0}{\lambda\sqrt{m}}|m\right) = -am\left(\frac{-L/2-s_0+l_p}{\lambda\sqrt{m}}|m\right)$ which leads to

$$s_0 = -\frac{1}{2}n_b l_p(m) \tag{D18}$$

with $n_b = 0, +1, +2, \ldots$ Plugging this result into Eq. $(D15)$ we have

$$L = 2\lambda\left(n_b 2\mathcal{K}\left(\frac{1}{m}\right) \mp \mathcal{F}\left(\arcsin\left(\sqrt{1 - \frac{m}{\mu}}\right)|\frac{1}{m}\right)\right) . \tag{D19}$$

Therefore, for a given value n_b we have two different solutions for m depending on the sign $\mp$. The case $n_b = 0$ corresponds to the portion of trajectory of b^- between the star and the circle in Fig. 16. One can make the same analysis as in the case $m < 1$. The solution is symmetric with $s_0 = 0$ but is unstable. It is a minimum of the curve $E(m, s_{0,-}(m))$ but a saddle point of the landscape $E(m, s_0)$. This solution does not exist for $L > L_{min}$.

For $n_b = +1, +2, ...$ Eq. $(D19)$ implies in both cases

$$l_p(\mu) \leq \frac{L}{n_b} \,, \tag{D20}$$

which leads to $1 < n_b < n_{b,\text{max}}$ with $n_{b,\text{max}} = \lfloor L/l_p(\mu) \rfloor$. The two solutions for a given n_b are not equivalent. The shapes with the positive sign in Eq.$(D19)$ corresponds to the case $-\pi/2 < \psi(-L/2) < 0$ and are unstable (see Appendix E). They are the critical shapes with two anti-twist-kinks (localized at both ends of the squeelix) on the top of the energy barrier that must be overcome to inject or expel one or both anti-twist-kinks.

Only the solution with the negative sign in Eq. (D19) corresponding to $0 < \psi(-L/2) < \pi/2$ leads to *stable* shapes that are therefore minima of the elastic energy. The shapes are such that the curvature inversion points are distributed in an equidistant manner within the squeelix (see main text for some shapes).

In Fig. 14 we observe that some extrema are not numbered. These extrema at position, say m_i, originate from our choice of the functional space. They do do not fulfill the boundary conditions Eq. (10) but instead satisfy $\delta\psi(L/2)\big|_{m_i} = \frac{\partial\psi(L/2)}{\partial m}\big|_{m_i}\delta m = 0$ so that $\delta E = 0$ in Eq. (A4) is still satisfied.

Appendix E: Stability analysis

To study the stability of the solutions (A15) which satisfy the Neumann boundary conditions (A5), we perform the second variation of the energy Eq. (A3)

$$\delta^2 E = C \int_{-L/2}^{L/2} \left(\tilde{\psi}(s)'^2 + V(s)\tilde{\psi}(s)^2 \right) ds \tag{E1}$$

with $V(s) = \frac{1}{\lambda^2}\left(2\sin^2\psi - 1 \right)$ and $\tilde{\psi} = \delta\psi$ a small variation around a solution (A15). Integrating Eq. (E1) by parts gives

$$\delta^2 E = C \left[\tilde{\psi}\frac{d}{ds}\tilde{\psi} \right]_{-L/2}^{L/2} + C \int_{-L/2}^{L/2} \tilde{\psi}\mathcal{L}\tilde{\psi}\, ds \,, \tag{E2}$$

where $\mathcal{L} = -\frac{d^2}{ds^2} + V(s)$ is a Lamé operator. We now distinguish the cases $m < 1$ and $m > 1$.

1. The revolving pendulum ($m < 1$)

Stability problems with fluctuations that satisfy the Neumann boundary conditions are discussed in Ref. [24]. In our case the Neumann boundary condition is a natural condition for the extremal energy configuration only. There is no external torque that would impose the Neumann conditions to the full twist $\psi(s)$. At finite temperature all fluctuations $\tilde{\psi}(s)$ around an extremal energy configuration are physically allowed and not only those with $\tilde{\psi}'(s) = 0$. Therefore, in our analysis we consider a general fluctuation which does not necessarily respect the Neumann boundary conditions. Doing so we will find the fluctuation $\tilde{\psi}(s)$ (around a particular solution of the Euler-Lagrange equation) that minimizes the second derivative of the energy $\delta^2 E$. When this minimum of $\delta^2 E$ is positive, the solution is stable with respect to any kind of fluctuation (in particular those respecting the Neumann conditions). When it is negative, the considered solution is unstable.

Starting with a fluctuation of the form $\tilde{\psi} \to \tilde{\psi} + \sigma s + \rho$ with $\tilde{\psi} = 0$ at the chain ends, Eq. (E2) becomes

$$\delta^2 E = C \left\{ A_1\sigma^2 + 2A_2\sigma\rho + A_3\rho^2 + \int_{-L/2}^{L/2} \left(2\sigma s V(s)\tilde{\psi} + 2\rho V(s)\tilde{\psi} + \tilde{\psi}\mathcal{L}\tilde{\psi} \right) ds \right\} \tag{E3}$$

with

$$A_1 = \int_{-L/2}^{L/2} s^2 V(s)ds + L \ , \tag{E4a}$$

$$A_2 = \int_{-L/2}^{L/2} sV(s)ds \ , \tag{E4b}$$

$$A_3 = \int_{-L/2}^{L/2} V(s)ds \ . \tag{E4c}$$

For given σ and ρ, we aim to minimize $\delta^2 E$. This amounts to solve the equation

$$\sigma s V(s) + \rho V(s) + \mathcal{L}\tilde{\psi} = 0 \tag{E5}$$

with $\tilde{\psi} = 0$ at the chain's ends. The solution of Eq. ($E5$) is a minimum if its second order fluctuation is positive. One thus has to find the sign of $\int_{-L/2}^{L/2} \bar{\psi}\mathcal{L}\bar{\psi}\,ds$, where $\bar{\psi}$ is the fluctuation of the fluctuation $\tilde{\psi}$. The Lamé operator has the eigenvalues 0, $\frac{1-m}{m}$, and $\frac{1}{m}$. Thus, the second order fluctuation is positive definite. The implicit dependence of this solution on the parameters σ and ρ is linear. It is thus a combination

$$\tilde{\psi}(s) = \alpha\tilde{\psi}^{(0)}(s) + \sigma\tilde{\psi}^{(1)}(s) + \rho\tilde{\psi}^{(2)}(s) \ . \tag{E6}$$

Then from Eq. (E5) we obtain

$$\mathcal{L}\tilde{\psi}^{(0)}(s) = 0 \ , \tag{E7}$$

$$sV(s) + \mathcal{L}\tilde{\psi}^{(1)}(s) = 0 \ , \tag{E8}$$

$$V(s) + \mathcal{L}\tilde{\psi}^{(2)}(s) = 0 \tag{E9}$$

with $\tilde{\psi}^{(i)}$ equal to zero at the boundaries. The first equation shows that $\tilde{\psi}^{(0)}(s) = dn\left(\frac{s-s_0}{\lambda\sqrt{m}}|m\right)$ is the zero mode of $\mathcal{L}$. Since $dn\left(\frac{s-s_0}{\lambda\sqrt{m}}|m\right)$ does not satisfy the boundary condition, we have $\alpha = 0$. To build the two other components $\tilde{\psi}^{(1)}$ and $\tilde{\psi}^{(2)}$ we first set

$$\varphi\left(\frac{s-s_0}{\lambda\sqrt{m}},m\right) = \frac{1}{1-m}\left[dn\left(\frac{s-s_0}{\lambda\sqrt{m}}|m\right)\mathcal{E}\left(am\left(\frac{s-s_0}{\lambda\sqrt{m}}|m\right)|m\right)\right. \tag{E10}$$

$$\left. -mcn\left(\frac{s-s_0}{\lambda\sqrt{m}}|m\right)sn\left(\frac{s-s_0}{\lambda\sqrt{m}}|m\right)\right]. \tag{E11}$$

The general solution of the second and the third equations (E8 -E9) are

$$\tilde{\psi}^{(1)}(s) = C_1 dn\left(\frac{s-s_0}{\lambda\sqrt{m}}|m\right) + C_2\varphi\left(\frac{s-s_0}{\lambda\sqrt{m}}|m\right) - s \ , \tag{E12}$$

$$\tilde{\psi}^{(2)}(s) = C_3 dn\left(\frac{s-s_0}{\lambda\sqrt{m}}|m\right) + C_4\varphi\left(\frac{s-s_0}{\lambda\sqrt{m}}|m\right) - 1 \ . \tag{E13}$$

To fix the coefficients C_i we take into account the boundary conditions $\tilde{\psi}^{(i)}(\pm L/2) = 0$. Using

$$\psi(-L/2) = am\left(\frac{-L/2-s_0}{\lambda\sqrt{m}}|m\right) = \pm\arcsin\sqrt{\frac{1}{m}-\frac{1}{\mu}} \ , \tag{E14}$$

$$\psi(L/2) = am\left(\frac{L/2-s_0}{\lambda\sqrt{m}}|m\right) = \begin{cases} \psi(-L/2) + n_a\pi & (\text{case}(a)) \\ -\psi(-L/2) + n_b\pi & (\text{case}(b)) \end{cases} \tag{E15}$$

(see Appendix D), we get for the case (a)

$$\tilde{\psi}_a^{(1)}(s) = -L\sqrt{\frac{\mu}{m}}\frac{\mathcal{E}(\psi(-L/2)|m) - \frac{1}{2}\sqrt{\mu m}\sin(2\psi(-L/2))}{\mathcal{E}(\psi(L/2)|m) - \mathcal{E}(\psi(-L/2)|m)}dn\left(\frac{s-s_0}{\lambda\sqrt{m}}|m\right) \ , \tag{E16}$$

$$+ L\sqrt{\frac{\mu}{m}}\frac{1-m}{\mathcal{E}(\psi(L/2)|m) - \mathcal{E}(\psi(-L/2)|m)}\varphi\left(\frac{s-s_0}{\lambda\sqrt{m}},m\right) - s$$

$$\tilde{\psi}_a^{(2)}(s) = \sqrt{\frac{\mu}{m}}dn\left(\frac{s-s_0}{\lambda\sqrt{m}}|m\right) - 1 \ , \tag{E17}$$

and for the case (b)

$$\tilde{\psi}_b^{(1)}(s) = -L\sqrt{\frac{\mu}{m}} \frac{\mathcal{E}\left(\psi\left(-L/2\right)|m\right) - \frac{1}{2}\sqrt{\mu m}\sin\left(2\psi\left(-L/2\right)\right)}{\mathcal{E}\left(\psi\left(L/2\right)|m\right) - \mathcal{E}\left(\psi\left(-L/2\right)|m\right) + \sqrt{\mu m}\sin\left(2\psi\left(-L/2\right)\right)} dn\left(\frac{s-s_0}{\lambda\sqrt{m}}\Big|m\right), \tag{E18}$$

$$+ L\sqrt{\frac{\mu}{m}} \frac{1-m}{\mathcal{E}\left(\psi\left(L/2\right)|m\right) - \mathcal{E}\left(\psi\left(-L/2\right)|m\right) + \sqrt{\mu m}\sin\left(2\psi\left(-L/2\right)\right)} \varphi\left(\frac{s-s_0}{\lambda\sqrt{m}}\Big|m\right) - s$$

$$\tilde{\psi}_b^{(2)}(s) = \sqrt{\frac{\mu}{m}} dn\left(\frac{s-s_0}{\lambda\sqrt{m}}\Big|m\right) - 1. \tag{E19}$$

In order to determine the sign of $\delta^2 E(\tilde{\psi})$ we use the decomposition (E6) to write

$$2\sigma s V(s)\tilde{\psi} + 2\rho V(s)\tilde{\psi} + \tilde{\psi}\mathcal{L}\tilde{\psi} =$$

$$\sigma^2 s V(s)\tilde{\psi}^{(1)} + \rho^2 V(s)\tilde{\psi}^{(2)} + \sigma\rho\left(s V(s)\tilde{\psi}^{(2)} + V(s)\tilde{\psi}^{(1)}\right). \tag{E20}$$

Replacing this equality in Eq. (E3), we get

$$\delta^2 E(\tilde{\psi}) = C\left\{\sigma^2 \tilde{A}_1 + 2\sigma\rho\tilde{A}_2 + \rho^2\tilde{A}_3\right\}. \tag{E21}$$

Then the stability conditions can be written

$$\tilde{A}_1 > 0, \tag{E22a}$$

$$\tilde{A}_3 > 0, \tag{E22b}$$

$$\tilde{A}_1\tilde{A}_3 - \tilde{A}_2^2 > 0, \tag{E22c}$$

where we have defined

$$\tilde{A}_1 = A_1 + \int_{-L/2}^{L/2} s V(s)\tilde{\psi}^{(1)} ds, \tag{E23a}$$

$$\tilde{A}_2 = A_2 + \frac{1}{2}\int_{-L/2}^{L/2}\left(s V(s)\tilde{\psi}^{(2)} + V(s)\tilde{\psi}^{(1)}\right) ds, \tag{E23b}$$

$$\tilde{A}_3 = A_3 + \int_{-L/2}^{L/2} V(s)\tilde{\psi}^{(2)} ds. \tag{E23c}$$

Using Eqs. (E8-E9) and the boundary conditions we obtain

$$\tilde{A}_1 = A_1 + \int_{-L/2}^{L/2} s V(s)\tilde{\psi}^{(1)}(s) ds$$

$$= \int_{-L/2}^{L/2} s^2 V(s) ds + \int_{-L/2}^{L/2} s\left(\mathcal{L} + \frac{d^2}{ds^2}\right)\tilde{\psi}^{(1)}(s) ds + L$$

$$= \int_{-L/2}^{L/2} s\left(\frac{d^2}{ds^2}\tilde{\psi}^{(1)}\right) ds + L$$

$$= \frac{L}{2}\left(\frac{d}{ds}\tilde{\psi}^{(1)}(-L/2) + \frac{d}{ds}\tilde{\psi}^{(1)}(L/2)\right) + L \tag{E24}$$

and in the same manner

$$\tilde{A}_2 = A_2 + \frac{1}{2}\int_{-L/2}^{L/2}\left(s V(s)\tilde{\psi}^{(2)} + V(s)\tilde{\psi}^{(1)}\right) ds$$

$$= \int_{-L/2}^{L/2} V(s) s ds + \frac{1}{2}\int_{-L/2}^{L/2}\left(s\left(\mathcal{L} + \frac{d^2}{ds^2}\right)\tilde{\psi}^{(2)} + \left(\mathcal{L} + \frac{d^2}{ds^2}\right)\tilde{\psi}^{(1)}\right) ds$$

$$= \frac{1}{2}\int_{-L/2}^{L/2}\left(s\frac{d^2}{ds^2}\tilde{\psi}^{(2)} + \frac{d^2}{ds^2}\tilde{\psi}^{(1)}\right) ds$$

$$= \frac{1}{2}\left(\frac{L}{2}\left(\frac{d}{ds}\tilde{\psi}^{(2)}(-L/2) + \frac{d}{ds}\tilde{\psi}^{(2)}(L/2)\right)\right) + \frac{1}{2}\left[\frac{d}{ds}\tilde{\psi}^{(1)}(s)\right]_{-L/2}^{L/2}, \tag{E25}$$

as well as

$$\tilde{A}_3 = A_3 - \int_{-L/2}^{L/2} V(s)\,\tilde{\psi}^{(2)} ds$$

$$= \int_{-L/2}^{L/2} V(s)\,ds + \int_{-L/2}^{L/2}\left(\mathcal{L} + \frac{d^2}{ds^2}\right)\tilde{\psi}^{(2)} ds = \left[\frac{d}{ds}\tilde{\psi}^{(2)}(s)\right]_{-L/2}^{L/2} . \tag{E26}$$

Now we have to distinguish between the cases (a) and (b) to check the stability conditions Eqs. (E22a-E22c). After calculating the different terms in $\tilde{A}_i$ and using the expression of $\tilde{\psi}^{(i)}_{a,b}(s)$ we arrive at

$$\tilde{A}_{1a} = LC_{2a}\frac{\sqrt{\mu}}{\lambda m} , \tag{E27a}$$

$$\tilde{A}_{2a} = -\frac{L}{2}\frac{\sqrt{\mu}}{\lambda}\sin\left(2\psi\left(-L/2\right)\right) , \tag{E27b}$$

$$\tilde{A}_{3a} = 0 , \tag{E27c}$$

and

$$\tilde{A}_{1b} = \frac{L}{\lambda}\left(\frac{L}{4}\frac{\mu}{\sqrt{m}}\sin\left(2\psi\left(-L/2\right)\right) + \frac{\sqrt{\mu}}{m}C_{2b}\right) , \tag{E28a}$$

$$\tilde{A}_{2b} = 0 , \tag{E28b}$$

$$\tilde{A}_{3b} = \frac{\sqrt{\mu}}{\lambda}\sin\left(2\psi\left(-L/2\right)\right) . \tag{E28c}$$

The conditions Eqs. (E22a-E22c) are never satisfied for the case (a) which thus corresponds to unstable solutions. This follows directly from Eq. (E22c) with $\tilde{A}_{3a} = 0$.

For the stability conditions of case (b) to be satisfied, we must have $\tilde{A}_{1b} > 0$ and $\tilde{A}_{3b} > 0$. For $\tilde{A}_{3b}$ this is true only if $\psi\left(-L/2\right) \in \left]0, \frac{\pi}{2}\right]$. For $\tilde{A}_{1b}$, we have to check the sign of C_{2b} which is the sign of $\mathcal{E}\left(\psi\left(L/2\right)|m\right) - \mathcal{E}\left(\psi\left(-L/2\right)|m\right)$. It is always positive because $\mathcal{E}(x,m)$ is a monotonically increasing function. Then $\psi'(s) > 0$ (as we have chosen $\omega_3 > 0$) leads to $\psi\left(\frac{L}{2}\right) > \psi\left(-\frac{L}{2}\right)$. Therefore, case (b) with $\psi(-L/2) > 0$ corresponds to stable solutions whereas all other cases are unstable.

2. The oscillating pendulum $(m > 1)$

In the case where $m > 1$ the twist ψ is a periodic function of s. We thus distinguish two cases.

Case (a)

The shape of the squeelix exhibits a certain number of waves or oscillations. In the following we will consider a chain of length L with one period $l_p = L$, and thus we choose $s = -L/2$ to $s = -L/2 + l_p = L/2$. We start with a perturbation of the form

$$\tilde{\psi}(s) = \cos\psi(s) . \tag{E29}$$

The second order variation of the energy, Eq. (E2), follows as

$$\delta^2 E = \left[-\frac{C}{\lambda\sqrt{m}}cn\left(\frac{s-s_0}{\lambda\sqrt{m}}\Big|m\right)sn\left(\frac{s-s_0}{\lambda\sqrt{m}}\Big|m\right)dn\left(\frac{s-s_0}{\lambda\sqrt{m}}\Big|m\right)\right]_{-L/2}^{L/2} + C\int_{-L/2}^{L/2}\tilde{\psi}\mathcal{L}\tilde{\psi}ds$$

$$= C\int_{-L/2}^{L/2} cn\left(\frac{s-s_0}{\lambda\sqrt{m}}\Big|m\right)\mathcal{L}cn\left(\frac{s-s_0}{\lambda\sqrt{m}}\Big|m\right)ds$$

$$= C\frac{(1-m)}{\lambda^2 m}\int_{-L/2}^{L/2} cn\left(\frac{s-s_0}{\lambda\sqrt{m}}\Big|m\right)^2 ds < 0 . \tag{E30}$$

All solutions of case (a) are thus unstable.

Case (b)

We now consider a chain which is longer than the period, *i.e.*, $s = -L/2$ to $s = -L/2 + L_p = s_1$ and a portion of the chain from $s = s_1$ to $s = L/2$. Choosing

$$\tilde{\psi} = dn\left(\frac{s - s_0}{\lambda\sqrt{m}}|m\right) , \tag{E31}$$

which is a zero eigenmode of $\mathcal{L}$, we have

$$\delta^2 E_{-L/2 \to s_1} = -C\frac{\sqrt{m}}{\lambda}\left[cn\left(\frac{s - s_0}{\lambda\sqrt{m}}|m\right) sn\left(\frac{s - s_0}{\lambda\sqrt{m}}|m\right) dn\left(\frac{s - s_0}{\lambda\sqrt{m}}|m\right)\right]_{-L/2}^{s_1} + C\int_{-L/2}^{s_1}\tilde{\psi}\mathcal{L}\tilde{\psi}ds = 0 . \tag{E32}$$

Thus

$$\begin{aligned}
\delta^2 E &= -C\frac{\sqrt{m}}{\lambda}\left[cn\left(\frac{s - s_0}{\lambda\sqrt{m}}|m\right) sn\left(\frac{s - s_0}{\lambda\sqrt{m}}|m\right) dn\left(\frac{s - s_0}{\lambda\sqrt{m}}|m\right)\right]_{s_1}^{\frac{L}{2}} + C\int_{s_1}^{\frac{L}{2}}\tilde{\psi}\mathcal{L}\tilde{\psi}ds \\
&= 2C\frac{\sqrt{m}}{\lambda}cn\left(\frac{-L/2 - s_0}{\lambda\sqrt{m}}|m\right) sn\left(\frac{-L/2 - s_0}{\lambda\sqrt{m}}|m\right) dn\left(\frac{-L/2 - s_0}{\lambda\sqrt{m}}|m\right) \\
&= 2C\frac{\sqrt{m}}{\lambda}\cos\left(\psi\left(-L/2\right)\right)\sin\left(\psi\left(-L/2\right)\right)\sqrt{1 - m\sin^2\left(\psi\left(-\frac{L}{2}\right)\right)} , \tag{E33}
\end{aligned}$$

where we have used the fact that $\psi'\left(-L/2\right) = dn\left(\frac{-L/2 - s_0}{\lambda\sqrt{m}}|m\right) = \sqrt{1 - m\sin^2\left(\psi\left(-\frac{L}{2}\right)\right)} = \omega_3 > 0$.

Since $\psi\left(-L/2\right) = \pm\arcsin\sqrt{\frac{1}{m} - \frac{1}{\mu}}$, one finds that solutions with $\psi\left(-L/2\right) < 0$ are unstable whereas solutions with $\psi\left(-L/2\right) > 0$ are stable.

---

[1] O. Kahraman, N. Stoop, and M. M. Müller, Fluid membrane vesicles in confinement, New Journal of Physics 14, 095021 (2012).
[2] N. Stoop, J. Najafi, F. K. Wittel, and M. Habibi, Packing of Elastic Wires in Spherical Cavities, Physical Review Letters 106, 214102 (2011).
[3] J. Guven and P. Vázquez-Montejo, Confinement of semiflexible filaments, Physical Review E 85, 026603 (2012).
[4] H. P. Hsu and P. Grassberger, Polymer confined between two parallel walls, The Journal of Chemical Physics 120, 2034 (2004)
[5] T. Sanchez, I. M. Kulić, and Z. Dogic, Circularization, photomechanical switching and a supercoiling transition of actin filaments, Physical Review Letters 104, 098103 (2010).
[6] J. Guven, D. M. Valencia, and P. Vázquez-Montejo, Environmental bias and elastic curves on surfaces, J. Phys. A: Math. Theor 47, 355201 (2014).
[7] G. H. M. van der Heijden, The static deformation of a twisted elastic rod constrained to lie on a cylinder, Proc. R. Soc. Lond. A457, 695 (2001).
[8] G. H. M. van der Heijden, A. R. Champneys, and J. M. T. Thompson, Spatially complex localisation in twisted elastic rods constrained to a cylinder, International Journal of Solids and Structures 39, 1863 (2002).
[9] G. H. M. van der Heijden, M. A. Peletier, and R. Planqué, Self-contact for rods on cylinders, Archive for rational mechanics and analysis 182, 471 (2006).
[10] G. H. M. van der Heijden, A. R. Champneys, and J. M. T. Thompson, Spatially complex localisation in twisted elastic rods constrained to lie in the plane, Journal of the Mechanics and Physics of Solids 47, 59 (1999).
[11] J. H. Maddocks, Stability of nonlinearly elastic rods, Archive for rational mechanics and analysis 85, 311 (1984).
[12] H. Mohrbach, A. Johner, and I. M. Kulić, Tubulin bistability and polymorphic dynamics of microtubules, Physical Review Letters 105, 268102 (2010).
[13] H. Mohrbach, A. Johner, and I. M. Kulić, Cooperative lattice dynamics and anomalous fluctuations of microtubules, European Biophysical Journal 41, 217 (2012).
[14] C. Lu, M. Reedy, and H. P. Erickson, Straight and curved conformations of FtsZ are regulated by GTP hydrolysis, Journal of Bacteriology 182, 164 (2000).
[15] S. M. Ferguson and P. De Camilli, Dynamin, a membrane-remodelling GTPase, Nat. Rev. Mol. Cell Biol. 13, 75 (2012).
[16] S. Asakura, G. Eguchi, and T. Iino, *Salmonella* flagella: *in vitro* reconstruction and over-all shapes of flagellar filaments, J. Mol. Biol. 16, 302 (1966).

[17] A. Volodin *et al.*, Imaging the elastic properties of coiled carbon nanotubes with atomic force microscopy, Physical Review Letters 84, 3342 (2000).

[18] S. M. Douglas, J. J. Chou, and W. M. Shih, DNA-nanotube-induced alignment of membrane proteins for NMR structure determination, Proc. Natl. Acad. Sci. U.S.A. 104, 6644 (2007).

[19] G. M. Nam, N. K. Lee, H. Mohrbach, A. Johner, and I. M. Kulić, Helices at interfaces, Europhysics Letters 100, 28001 (2012).

[20] M. Nizette and A. Goriely, Towards a classification of Euler-Kirchhoff filaments. Journal of Mathematical Physics 40, 2830 (1999).

[21] O. Kahraman, H. Mohrbach, M. M. Müller, and I. M. Kulić, Confotronic dynamics of tubular filaments, Soft Matter 10, 2836 (2014).

[22] N. Chouaieb, A. Goriely, and J. H. Maddocks, Helices, Proc. Natl. Acad. Sci. U.S.A. 103, 9398 (2006).

[23] Abramowitz M and Stegun IA 1970 *Handbook of Mathematical Functions* 9th edn. (Dover, Mineola, NY).

[24] R. S. Manning, Conjugate points revisited and Neumann-Neumann problems, SIAM review 51, 193 (2009).

[25] J. F. Currie, J. A. Krumhans, A. R. Bishof, and S. E. Trullinger, Statistical mechanics of one-dimensional solitary-wave-bearing scalar fields: exact results and ideal-gas phenomenology, Physical Review B 22, 477 (1980).

[26] P. Gosselin, H. Mohrbach, I. M. Kulić, and F. Ziebert, On complex, curved trajectories in microtubule gliding, Physica D 318-319, 105 (2016).

[27] G. Domokos, P. Holmes, and B. Royce, Constrained euler buckling, Journal of Nonlinear Science 7, 281 (1997).

[28] R. S. Manning and G. B. Bulman, Stability of an elastic rod buckling into a soft wall, Proceedings of the Royal Society of London A: Mathematical, Physical and Engineering Sciences 461, 2423 (2005).

[29] B. Nöding and S. Köster, Intermediate Filaments in Small Configuration Spaces, Physical Review Letters 108, 088101 (2012).

[30] J. H. Maddocks, Stability and folds, Archive for Rational mechanics and Analysis 99, 301 (1987).

[31] I. M. Kulić, H. Mohrbach, V. Lobaskin, R. Thaokar, and H. Schiessel, Apparent Persistence Length of Bend DNA Physical Review E 72, 041905 (2005).

[32] I. M. Kulić, H. Mohrbach, R. Thaokar, and H. Schiessel. Equation of state of looped DNA, Physical Review E 75, 011913 (2007).

[33] Note that a generalization of this model consists of considering two bending moduli which introduces an anisotropy and is, for instance, closer to DNA. This is beyond the scope of this paper but may be an interesting starting point for future work.